Nanoparticle mediated in vitro and in vivo CRISPR base correction of LCA16 causing nonsense mutation rescues Kir7.1 channel function

Authors: Meha Kabra[1, 2,*], Pawan K Shahi[1, 2,*], Yuyuan Wang[3, 4], Divya Sinha[2, 5], Allison Spillane[1], Gregory A. Newby[6, 7], Shivani Saxena[2, 3], Kimberly Edwards[2, 5], Cole Theisen[2, 5], David Gamm[2, 8], David R. Liu[6, 7,9], Shaoqin Gong[2, 3], Krishanu Saha[2, 3], Bikash R. Pattnaik[1,2,8, **]

Meha Kabra and Pawan K Shahi share equal authorship.

Author affiliations: [1]Department of Pediatrics, University of Wisconsin-Madison, Madison, WI, United States. [2]McPherson Eye Research Institute, University of Wisconsin-Madison, Madison, WI, United States. [3]Department of Biomedical Engineering, Wisconsin Institute of Discovery, University of Wisconsin-Madison, Madison, WI, United States. [4]Department of Materials Science and Engineering, University of Wisconsin-Madison, Madison, WI, United States. [5]Waisman Center, University of Wisconsin-Madison, Madison, WI, United States. [6]Merkin Institute of Transformative Technologies in Healthcare, Broad Institute of Harvard and MIT, Cambridge, MA, United States. [7]Howard Hughes Medical Institute, Harvard University, Cambridge, MA, United States. [8]Department of Ophthalmology and Visual Sciences, University of Wisconsin-Madison, Madison, WI, United States. [9]Department of Chemistry and Chemical Biology, Harvard University, Cambridge, MA, United States.

Corresponding author: Correspondence should be addressed to Dr. Bikash Pattnaik, University of Wisconsin-Madison, Madison, WI 53706, USA. Email: pattnaik@wisc.edu, Phone: (608)265-9486 (Off), (608)262-0991 (Lab) | Fax: (608)262-6298.

Abstract

Lebers Congenital Amaurosis (LCA16) is caused by point mutations in *KCNJ13* gene, which encodes for an inward-rectifying potassium channel, Kir7.1. A nonsense mutation, W53X (c.158G>A), leads to premature truncation of protein which makes retinal pigmented epithelial (RPE) non-functional. Molecular mechanism studies revealed a compromised membrane potential, altered subretinal ionic homeostasis, and loss in phagocytic activity caused autosomal recessive childhood blindness. Since all reported mutations in *KCNJ13* gene are single base change, CRISPR base editing offers a potential means to correct gene function endogenously and restores the channel function permanently. Further, base editing is free of double-stranded breaks and homology-directed repair (HDR) to generate minimal to no off-targets and indels. Here, we report the silica-nanoparticle (SNP) mediated delivery of an Adenosine CRISPR base editor (ABE8e) mRNA and single-guide RNA for the correction of *KCNJ13-W53X* (c.158G>A) mutation in an induced pluripotent stem cell-derived (iPSC)-RPE model of LCA16. We demonstrated that, unlike CRISPR-Cas9 mediated gene editing, base editing by ABE8e can efficiently and precisely correct the gene mutation in post-mitotic cells like RPE. We observed a higher editing efficiency in LCA16-patient-derived fibroblasts (47.38% ± 1.02) than iPSC-RPE (16.90% ± 1.58) with no detectable off-target activity at the predicted sites. The SNP-mediated ABE8e delivery and correction of W53X mutation in iPSC-RPE restored the Kir7.1 channel activity with no noticeable toxicity to cells. Restoration of channel function in the edited cells was comparable to a wild-type phenotype, which is a prime requisite for vision restoration in LCA16 patients. Subretinal injections of SNPs decorated with all-trans retinoic acid (ATRA) ligand with a payload of ABE8e and mouse-specific sgRNA in LCA16 mice (with no ERG phenotype) showed specific delivery only to RPE. We observed marginal recovery of ERG generated from the correction of the W53X allele at the injection site with no further degeneration of RPE. These findings provide a foundation and a proof-of-concept to transition from bench to bedside and support its further development for treating pediatric blindness using a safer mode of SNP-mediated delivery of CRISPR base editors.

Keywords: CRISPR Base editing, gene correction, *KCNJ13* loss-of-function nonsense mutation, Kir7.1 ion channel, Leber congenital amaurosis 16 (LCA16), inherited retinal blindness, induced pluripotent stem cells- retinal pigment epithelium (hiPSC-RPE).

Introduction

Leber's congenital amaurosis (LCA16; OMIM#614186) is one of the severe forms of autosomal recessive inherited retinal dystrophies (IRDs), caused due to a non-functional Kir7.1 ion channel in the apical process of the retinal pigmented epithelium (RPE)[1] cells which is translated from a mutant *KCNJ13* gene (location#2q37.1, OMIM#603208)[2]. The Kir7.1 channel, composed of 360 amino acids, primarily controls K^+ homeostasis in the subretinal space to regulate processes such as phototransduction and phagocytosis by RPE. Several missense and nonsense loss-of-function mutations have been reported in *KCNJ13*, which abolish K^+ conductance due to altered structure, assembly, and trafficking of Kir7.1 protein[3-9]. Earlier, we reported an LCA16 patient with a homozygous nonsense *KCNJ13* mutation (W53X, c.158G>A) and showed the effect of Kir7.1 C-terminus truncation on altered trafficking and K^+ conductance[10]. We further validated the clinical LCA16 electroretinogram (ERG) phenotype in mice via targeted suppression of Kir7.1 using siRNA[11].

Currently, there is no available therapy for LCA16 in the clinic. A disease-in-a-dish induced pluripotent stem cells RPE (LCA16 iPSC RPE) model from the W53X patient was developed and characterized to establish the potential of therapies like translational readthrough inducing drugs (TRIDs) and AAV-gene augmentation for the treatment of childhood blindness[12]. However, limitations such as AAV-Gene therapy provoked innate and adaptive immune responses and short-term efficacy as the underlying mutation is not corrected challenges its clinical use. TRIDs are involved in protein correction, which is transient and may introduce another missense mutation at a premature truncation site instead of a WT amino acid. CRISPR/Cas9 mediated gene manipulations can correct an endogenous gene and offer a permanent change in the genome but also poses several challenges in restoring an ion channel protein. Unintended off-targets and indels at the on-target allele due to double-stranded breaks can change the allelic composition of a cell affecting the multimeric protein assembly and making even the correctly monoallelic edited cell non-functional[13]. HDR is highly inactive in non-dividing cells like RPE and may have lower efficiency in these RPE[14-16].

The challenges as mentioned above prompted us to use CRISPR base editing, which allows highly efficacious and precise correction of point mutations. CRISPR BE uses a modified version of Cas9 (Cas9 nickase, nCas9) fused to either adenosine deaminase (A>G change) in Adenosine base editors (ABEs) or cytosine deaminase (C>T change) in Cytosine base editors (CBEs) along with a guide RNA (sgRNA) and a protospacer adjacent motif (PAM). BE is an active DNA repair system independent of HDR. These BEs deaminase the single base at the targeted catalytic window of activity of 4-8bp from the PAM sequence and, therefore, create a myriad open possibility of correcting point mutations without generating excess undesired on-target/off-target by-products[17]. The ability to permanently fix the recessive loss-of-function *KCNJ13* point mutations could offer comprehensive clinical benefits to LCA16 patients.

Several base editing strategies could be designed using higher fidelity base editors with different delivery modes for a specific *KCNJ13* mutation. We used an efficient nanoplatform mode to deliver BEs/sgRNA instead of AAV vectors due to several published reports questioning its genome-wide integration and genotoxic effects [18-21]. Unlike AAVs, which also have limited packaging capacity, nanoparticles can be engineered to package a wide range of sizes and shapes. They can be used to deliver the biologics (DNA/RNA/protein) in a controlled released manner [22-24]. Recently reported silica nanoparticles (SNPs) decorated all-*trans*-retinoic acid (ATRA) or GalNAc showed tissue-specific delivery to RPE cells via subretinal injection and liver cells via intravenous injection, respectively. These SNPs successfully delivered the CRISPR tools in their active forms to the desired editing site safely and demonstrated the successful genome editing outcomes in murine RPE and liver cells[24].

In the present study, we explored the feasibility of correcting a *KCNJ13* point mutation endogenously in vitro and an in vivo LCA16 model by encapsulating the CRISPR tools in SNPs and evaluated the system's efficacy. We first characterize the phenotypic consequences of CRISPR/Cas9 and HDR-mediated gene editing in iPSC-RPE^{W53X}, in which the lentiviral approach was used to deliver sgRNA and Cas9. In contrast, the donor sequence was delivered via SNPs. To overcome the challenges of Cas9-gene editing, we then elucidated the potential of CRISPR base editing in our in vitro models, LCA16-W53X-fibroblasts, and

iPSC RPE^{W53X} cells and in vivo LCA16 disease models. The use of different cell lines demonstrated that the approach is well suited for an ex vivo cell therapy using autologous base corrected LCA16 fibroblast cells after their reprogramming and differentiation to RPE, in patients where RPE degenerates and for in vivo base editing of mature RPE. To evaluate base editing in the mouse model of LCA16, we selected the heterozygous (*Kcnj13*$^{W53X/+}$) mice with normal ERG phenotype as homozygous mice (*Kcnj13*$^{W53X/W53X}$) do not survive and die at postnatal day 1 (P1). We used a tissue-specific approach and disrupted the WT allele only in the retina of the adult mice via subretinal injection of CRISPR/Cas9 along with a specific sgRNA targeting only the WT allele. The loss of ERG confirmed the true LCA16 phenotype in the eyes of these adult mice. These mice (*Kcnj13*$^{W53X/-}$) were used to evaluate the activity of ABE8e mRNA along with a mouse-specific sgRNA targeting the W53X location. The treated *Kcnj13*$^{W53X/-}$ mice with ERG readout above the baseline of WT-allelic disruption would represent the phenotypic restoration of Kir7.1 function as an outcome of successful base editing.

Methods

1. **Ethical guidance and animal protocols**

   All work with LCA16 patient-derived cells (fibroblasts, iPSCs, and iPSC-RPE) was carried out in accordance with institutional, national, and international guidelines and approved by the University of Wisconsin-Madison's institutional review board and Stem Cell Research Oversight Committee. The animal protocols were in accordance with the ARVO Statement for use in ophthalmic and vision science research and approved by the University of Wisconsin school of Medicine and Public Health Animal Care and Use Committee (ACUC).

2. **HEK Flp-In™ 293 stable cells with GFP tagged WT and W53X Kir7.1 expression**

   HEK Flp-In™ 293 host cells (ThermoFisher Scientific#R75007, MA), generated using a pFRT/lacZeo target site vector, were used to express GFP-tagged Kir7.1 (WT and W53X). These cells contain a single Flp Recombination Target (FRT) site at a transcriptionally active genomic locus to allow stable integration of GFP-tagged human *KCNJ13* sequence (WT and W53X). As these cells express the Zeocin™ gene under SV40 early promoter, a complete D-MEM high glucose media [10% FBS, 1% Pen-Strep, 2mM L-glutamine] containing 100 µg/ml Zeocin™ was used for maintenance. GFP-WT and GFP-W53X *hKCNJ13* gene sequence was integrated into the genome of these cells based on the manufacturer's guidelines. Briefly, the cells were co-transfected with FLP-In™ expression vector (pcDNA5/FRT) containing GFP-tagged *hKCNJ13* sequence (WT or W53X), created by in-fusion cloning and pOG44 recombinase expression plasmid. The pOG44 plasmid with constitutive expression of the Flp recombinase under CMV promoter mediates the homologous recombination between the FRT sites of host cells and the expression vector such that the construct from the vector is inserted into the cell-genome at the FRT site. This insertion brings the Hygromycin B resistance gene in the frame, inactivates the zeocin fusion gene, and expresses the gene of interest under CMV promoter. 48 hours post-co-transfection, the cells were passaged at 25% confluency to select stable transfectants in 200 µg/ml of Hygromycin B. The Hygromycin B resistant cell clones (n=15-20) were picked, maintained in 100 µg/ml Hygromycin B, and further expanded for their characterization by genotyping (Sanger sequencing) and protein expression (immunocytochemistry). The primers used for in-fusion cloning and Sanger sequencing are listed in Supplementary Table 1.

3. **Patient's specific fibroblasts and iPSC RPE cell culture and maintenance**

   Fibroblasts derived from patient skin biopsy were cultured and maintained in complete DMEM high glucose media containing 10% FBS and 1% Pen-Strep at 37 °C with 5% CO_2. Induced pluripotent stem cells (iPSCs) were cultured on Matrigel and differentiated to iPSC-RPE using an approach similar to that previously described (Shahi et al. AJHG 2019; Sinha et al., AJHG 2020). Briefly, on D0 of differentiation, iPSCs were lifted using ReLeSR (Stem Cell Technologies; Cat# 05872) to generate embryoid bodies (EBs). The EBs were maintained overnight in mTeSR+ containing 10 µM ROCK inhibitor (R&D Systems; Cat# Y-27632). Then, over the next three days, the EBs were gradually transitioned to Neural Induction Media (NIM; DMEM: F12 1:1, 1% N2 supplement, 1x MEM nonessential amino acids (MEM NEAA), 1x GlutaMAX, and 2 µg/ml heparin (Sigma)). On D7, EBs were plated on Nunc 6-well plates coated with Laminin (ThermoFisher Scientific; Cat# 23017015), and on D16, neurospheres were mechanically lifted. Remaining adherent cells were transitioned to in retinal differentiation media (RDM; DMEMF12 (3:1), 2% B27 without retinoic acid, 1% antibiotic-antimycotic solution) and allowed to differentiate to RPE. For the first four media changes, RDM was supplemented with 10 µM SU5402 and 3 µM CHIR99021. After >60 days of differentiation, iPSC-RPE cells were purified as described by Sharma et al. and cultured on the desired surface[25].

4. **Silica-nanoparticles (SNPs) for Adenosine base editing and CRISPR/Cas9 gene editing**

   We used a recently reported safe and efficient nanoplatform to deliver the CRISPR gene editing and base editing components[24]. Glutathione-responsive silica nanoparticles of ~50 nm were synthesized via disulfide crosslinking. SNPs were synthesized using a water-in-oil microemulsion method. For a typical SNC synthesis using 1 ml organic solution, the oil phase was prepared by mixing Triton X-100 (885 µL) with hexanol (0.9 mL) and cyclohexane (3.75 mL). An aliquot of aqueous solution (25 µL) containing the desired payload (base editor mRNA + sgRNA, total concentration of nucleic acid is 2 mg/mL) was mixed with the

silica reagents: TEOS (4 μL), BTPD (6 μL) and N-(3-(triethoxysilyl) propyl)-1H-imidazole-4-carboxamide (TESPIC, 1 mg). The synthesis of TESPIC was reported previously[24]. This mixture was homogenized by pipetting and then added to the oil phase (1 mL). The water-in-oil microemulsion was formed by vortexing for 1 min. Under vigorous stirring (1,500 rpm), an aliquot of 30% aqueous ammonia solution (4 μL) was added, and the water-in-oil microemulsion was stirred at 4 °C for 12 h to obtain unmodified SNPs. Acetone (1.5 mL) was added to the microemulsion to precipitate the SNPs. The precipitate was recovered by centrifugation and washed twice with ethanol and three times with ultrapure water. The purified SNPs were collected by centrifugation. The as-prepared, unmodified SNP was re-dispersed in ultrapure water (1 mL). For Surface modification, mPEG-silane (for the synthesis of SNP-PEG without ATRA, or a mixture of mPEG-silane + silane-PEG-NH_2 (molar ratio of mPEG-silane: silane-PEG-NH_2 = 8:2, for the synthesis of SNP-PEG-NH_2) was added to the above-mentioned SNP suspension. The total amount of PEG is 10 wt% of SNP. The pH of the suspension was adjusted to 8.0 using a 30% aqueous ammonia solution. The mixture was stirred at room temperature for 4 h. The resulting SNPs were purified by washing with ultrapure water three times and concentrated with Amicon® Ultra Centrifugal Filters (Millipore Sigma, USA). ATRA was conjugated onto SNP via EDC/NHS catalyzed amidation. Payload-encapsulated SNP-PEG-NH_2 (0.5 mg) WAS re-dispersed in 1 mL DI water. EDC (7.5 μg), NHS (4.5 μg), and a DMSO solution of ATRA (6 μg in 5 μL DMSO) were added to the above solution. The solution was stirred at room temperature for 6 h, and then the resulting SNP-PEG-ATRA was washed with water three times and collected and concentrated with Amicon Ultra Centrifugal Filters.

5. **The sgRNA design**

The sgRNAs targeting W53X location in human and mouse *Kcnj13* gene were designed using Benchling (https://www.benchling.com), and the one with the highest on-target score (human; 65.7 and mouse; 57.1) and the lowest off-target score (human; 56.8 and mouse; 56.8) were selected for the base editing. The chemically modified form of these sgRNAs (human; G*C*G*CUAGCGUUGGAUGAUGU and mouse; G*C*G*CUAGCGCUGGAUGAUGC) were ordered from the Synthego (CA, USA).

6. **Generation of the lentiviral vector for Cas9 mediated gene editing**

Lentivirus was manufactured for Cas9-mediated editing as provided in Gándara, Carolina et al. (2018). Briefly, the HEK293 cells were plated and ready for transfection at 70% confluence, about 24 h after plating. Target plasmid was transfected along with packaging gene plasmids pMD2.G and psPAX2. The target vector plasmid contains the LCA transgene with expression driven by an EF-1α promoter. Cell culture supernatant was collected from HEK293 after transfection and was concentrated via gradient and centrifugation. A functional titer was performed to check the concentrated yield, between 10^7 and 10^{10} particles/mL.

7. **Gene editing in iPSC-RPE by lentiviral transduction (Cas9 and sgRNA delivery) and SNP (ssODN delivery)**

For our attempt to edit the *KCNJ13* gene carrying a W53X nonsense mutation, we used viral transduction to deliver cas9 and a sgRNA (TAATGGACATGCGCTAGCGT) to the matured iPS-RPE cells. Lentiviral vectors specifically designed for this purpose, lentiCRISPR v2-mCherry (Addgene plasmid # 99154), a gift from Agata Smogorzewska, were used and the annealed sgRNA oligonucleotides were cloned into it using the BsmB1 enzyme digestion. The sgRNA's successful integration was confirmed by DNA sequencing with the primer 5′-GGACTATCATATGCTTACCG-3′ for the U6 promoter, which also drives its expression. Using the previously described method, lentivirus was generated in-house. This lentivirus was used to transduce matured-iPS-RPE cells to express Cas9, sgRNA, and the reporter gene mCherry, allowing easy identification of the transduced cell. After 6 hours of viral transduction, 15ug of ssODN-ATTO488 (GATGCTTGGGG**G**ATCCTAATGGA**T**ATGCGCT**G**GCGTTGGATGATGTT**A**GTCTTTTCTGCTTC T, the bold letters show the wobble changes) was delivered to the cells using silica nanoparticles and incubated for 48 hours. The cells were examined for red and green fluorescent markers, and when they were found to be expressed, the monolayer cells on the transwells were dissociated into a single cell by papain digestion and subjected to patch-clamp studies.

8. **Base editing in Kir7.1-HEK293 stable cells by electroporation**
   The HEK293 stable cells expressing GFP-W53X-Kir7.1 were subcultured 24 hours prior to nucleofection at 70% confluency. The adenosine base editor mRNA (ABE8e-spCas9-NG, 3 µg)[26] and protein (ABE8e, 3 µg) as ribonucleoprotein (RNP) complex with the guide RNA (100 µM) were used to edit W53X mutation. For base editing, $1x10^5$ cells were electroporated using the FS-100 program in Lonza 4D nucleofector according to the manufacturer's guidelines. Post-electroporation, cells were seeded in a 6-well plate and maintained in 100 µg/ml Hygromycin B for further analysis.
9. **BE in LCA16-patient's specific fibroblasts and iPSC-RPE by SNPs**
   The W53X-LCA16-patient's specific fibroblasts were sub-cultured a day before treatment. For base editing, ABE mRNA (ABE8e-spCas9-NG, 3 µg) and sgRNA (100 µM) were delivered to fibroblasts using SNPs. 5 days post-treatment, DNA was isolated for genomic analysis. For base editing in iPSC-RPE, the cells were first seeded in a 96-well plate at a density of 50,000 cells per well in RDM containing 10% FBS and 10 µM ROCK inhibitor (R&D Systems; Cat# Y-27632). On Day 2, the media was switched to RDM containing 2% FBS. On day 3 post-seeding, ABE mRNA (3 µg) and sgRNA (100 µM) were delivered to the cells using SNPs in RDM. the iPSC-RPE monolayer was dissociated 2 days post-treatment with SNP-ABE. Cells were seeded on transwell inserts and also collected for genomic DNA analysis. iPSC-RPE cells transitioned to transwell inserts were cultured for 4-6 weeks to get a polarized monolayer of RPE and subsequently analyzed for Kir7.1 channel function by whole-cell patch-clamp approach. Untreated cells were used as references.
10. **Base editing in mice**
    C57BL/6J male and female mice (WT, W53X) were housed at the animal facility at UW Madison (Madison, WI) under a 12-hour light-dark cycle at a controlled temperature (25±5 °C) and humidity (40–50%). Genotyping of the mice was performed using standard PCR methods with the primers listed in supplementary table 2 followed by digestion with restriction enzyme NheI (Anza# IVGN0066, ThermoFisher). W53X mutation creates a restriction site for NheI, and therefore, W53X allele resulted in two (212 bp and 302 bp) fragments while the WT allele only one (514 bp) fragment (Supplementary figure 1). As homozygous W53X mice do not survive, we specifically knock down the WT-*Kcnj13* allele using CRISPR/Cas9 in the eyes of W53X-het mice to silence the Kir7.1 expression mimicking the LCA16 phenotype. ERG was done to confirm the loss of function, and the mice with reduced or no c-wave were used for the base editing of the W53X-*Kcnj13* allele. A subretinal injection (2 µl) with 3 µg of the base editor (ABE8e-spCas9-NG) and W53X-targeting sgRNA (100 µM) complexed with ligand (ATRA, all-trans retinoic acid) coated SNPs- was performed in mice (n=5 eyes). GFP mRNA (1 µg) was used in the complex preparation to visualize the site of injection and spread of SNPs in RPE. PBS or SNP-ATRA injected eyes were used as reference. 5 days post-injection, DNA was isolated from the optic cup of these mice for genomic analysis.
11. **On-target analysis by deep sequencing**
    Treated and untreated cells were dissociated using enzymatic treatment (Accutase/Papain) according to manufacturer's instructions for genomic analysis. From the HEK293 stable cells, total RNA (Qiagen#74134) was isolated, and reverse transcribed to cDNA (ThermoFisher#4368814), and subsequently amplified for on-target analysis using *KCNJ13* Illumina-specific primers (Supplementary Table 3). From fibroblasts, iPSC-RPE and mouse optic cup, genomic DNA was isolated according to manufacturer's guidelines (Quick-DNA™ Miniprep plus kit# D4069) and quantified using Nanodrop 2000 or Qubit (Thermo Fischer). For deep sequencing of the *KCNJ13* locus, genomic DNA was amplified using Illumina specific primers with adapter sequences (amplicon size ~150bp) (Supplementary Table 3). Unique indexes (i7 and i5) were ligated to each custom amplicon by PCR (amplicon size 250bp), and the indexed amplicons were pooled and purified using AMPure XP beads (Beckman Coulter#A63881). The indexed library was run on an illumina MiniSeq instrument, with a read length of 150bp. Deep sequencing data were analyzed using RGEN Cas-analyzer[27] (http://www.rgenome.net/cas-analyzer/)) and CRISPResso2[28] (https://crispresso.pinellolab.partners.org/submission) software.
12. **Off-target analysis by deep sequencing**

The potential off-target sites for the hW53X-sgRNA were identified by an in-silico tool, Cas-OFFinder (http://www.rgenome.net/cas-offinder/). The parameter used were an NG/NGG/NAG PAM, with or without DNA/RNA bulge (bulge size=1) and with up to 4 mismatches to the sgRNA sequence (Supplementary Table 4, Supplementary Figure 1). From the treated and untreated stable cells, fibroblasts and iPSC-RPE, gDNA was isolated and amplified using primers specific to off-target sites. All the primer sequences are listed in Supplementary Table 5. The deep sequencing and data analysis were performed as mentioned above.

13. rhAmp off-target analysis in W53X mice

As the genomic DNA yield from the mouse optic cup was too low to amplify all the off-target separately, we used a highly efficient RNase H2-dependent (rhAmp) PCR technique that can amplify different targets in a single PCR reaction. Amplification and sequencing run were performed according to manufacturer's instructions. Briefly, the rhAmpSeq CRISPR panel was designed using the IDT-designing tool for the potential off-targets of mW53X-sgRNA identified using Cas-OFFinder (Supplementary Table 6). Amplicon library was prepared using rhAmpSeq CRISPR Library Kit (IDT#10007317) and rhAmpSeq i5 and i7 index primers. The purified library was sequenced on an Illumina platform. Sequencing analysis was performed using IDT-rhAMP CRISPR analysis tool (https://www.idtdna.com/site/analysislab).

14. Immunocytochemistry

Kir7.1 protein expression was assessed in the pool of W53X-mutant, WT, and base edited HEK293 stable cells by immunocytochemistry as described earlier[12]. As the protein is GFP tagged, GFP mouse monoclonal primary antibody (Cell Signaling#2955, 1:250) was used to detect Kir7.1 protein expression in the cells. Sodium Potassium ATPase rabbit monoclonal primary antibody (Thermo Fisher#ST0533, 1:500) was used to label the cell membranes. Alexa fluor-594 conjugated Donkey anti-Rabbit (Proteintech#SA00006.8, 1:500) and Alexa fluor-488 conjugated Donkey anti-Mouse (Proteintech#SA00006.5, 1:500) secondary antibodies were used. DAPI was used as a nuclear counterstain. Immunostained cells were imaged on a confocal microscope (Nikon C2 Instrument).

15. Electrophysiology assay

An automated patch clamp (Q Patch II, Sophion, Denmark) was used to measure the whole-cell current from the HEK^{WT}, $HEK^{W53X,}$ and $HEK^{W53X\text{-}BE}$ stable cells as described earlier[29]. Briefly, the cells were grown in a T75 flask for 48-72 hours and then detached gently using Detachin™. The cells were centrifuged at 90 g for 1 min and resuspended in serum-free media containing 25 Mm HEPES. The cells [3 M/ml] were kept on instrument's shaker for 20 mins prior to the experiment. 48 cells were recorded in parallel on single-hole disposable Qplates with individual amplifiers. A pressure protocol was used to achieve cell positioning (-70 mbar), Giga seal (-75mbar), and whole-cell configuration (5 pulses with -50 mbar increment between the pulses, first pulse of -250 mbar). The current was recorded in response to voltage-clamp steps from the holding potential (-10mV) to voltages between -140mV and +40mV (Δ=10mV). More than 70% of the cells completed the experiment. The cells in which the stability was compromised during the experiment were judged by the leak current and excluded from the analysis. The extracellular solution contained (in mM): 135 NaCl, 5 KCl, 10 HEPES, 10 glucose, 1.8 $CaCl_{2,}$ and 1 $MgCl_{2,}$ pH adjusted to 7.4 and osmolarity 305 mOsm. The intracellular solution contained (in mM) 30 KCl, 83 K-gluconate, 10 HEPES, 5.5 EGTA, 0.5 $CaCl_2$, 4 Mg-ATP, and 0.1 GTP, pH adjusted to 7.2 and osmolarity 280 mOsm. In an alternative external solution, NaCl was replaced with RbCl [140 mM] and used as an enhancer of Kir7.1 current. The data was analyzed using Sophion Analyzer v6.6.44. Whole-cell manual patch-clamp recording of base edited hiPS-RPE cells was performed according to the standard protocol described elsewhere[10].

16. Electroretinography (ERG) in mice

ERG was performed in mice using a standard protocol described elsewhere[11], before and after the base editing to evaluate the function of the retina. Briefly, the mice were dark-adapted overnight prior to ERG. ERG signals were captured in full darkness using an Espion Ganzfeld full-field system (Diagnosys LLC, Lowell, MA). When using an ERG electrode, a drop of 2% hypromellose solution to the eye in order to keep the cornea wet and make electrical contact. For a and b-wave, the eyes were exposed to a series of flash intensities (0.03 to 30 cd.s/m2) using ganzfeld dome for 400 ms with a 2 s interval between each flash. For c-wave, the eyes were exposed to 25 cd.s/m2 for 4 s. Animals were subjected to ERG every 2 weeks,

and data acquired were analyzed with Espion software (Diagnosys LLC, Lowell, Massachusetts) and Origin2018b from. Origin2018b (OriginLab Corp., MA).

17. Statistical analysis

The data analysis was done using Origin software (Origin 2020, OriginLab Corporation, Northampton, MA, USA) and expressed as mean ± the standard error. Two-tailed unpaired Student's *t*-test was used to determine the statistical differences, and a $p < 0.05$ was considered significant. Final figures were assembled using Adobe Photoshop and illustrator 2020.

Results

1. CRISPR-Cas9 Gene editing corrects W53X mutation in iPSC RPE^{W53X} at lower efficiency

We used LentiCRISPRv2- mCherry, a lentiviral vector-based CRISPR/Cas9 delivery system expressing target sgRNA, Cas9 nuclease, and a mCherry reporter. A lenti-based approach was used because iPSC RPE cells are difficult to transfect to deliver the gene-editing tools like Cas9 RNPs and mRNA. Also, our previous studies showed success in delivering the open reading frame (ORF) of the gene using the lentivirus[12]. The delivery of the editing machinery was confirmed by the expression of mCherry in transduced iPSC-RPE^{W53X} cells. Visualization of GFP fluorescence similarly confirmed the delivery of the ssODN-ATTO488 donor sequence by silica nanoparticles. Patch-clamp analysis of cells expressing both mCherry and GFP revealed a normal Kir7.1 current with the inward current of -101.1 ± 35.54 pA at -150 mV, which is also being potentiated by the rubidium (Rb^+), a known activator of Kir7.1 current. The Rb^+ ion increased the Kir7.1 inward current by 7-fold to -713.5 ± 92.97 pA. As the electrophysiology assay was done in the pool of edited cells, it was difficult to determine the genetic background of the recovered cells. The recovery could be due to the corrected WT allele or indels created at DSBs. In addition to the viral delivery, non-viral delivery using nanoplatform like polyplexes and siMOF particles were utilized to deliver 12ug RNP payloads to iPSC-RPE^{W53X} cells. These cells showed a low level of editing by HDR, ranging from 2.5% to 7.4% (Supplementary Figure 3), which was identified based on the silent changes introduced in the ssODN. The absence of the reporter marker prevented measurements from being performed on these cells.

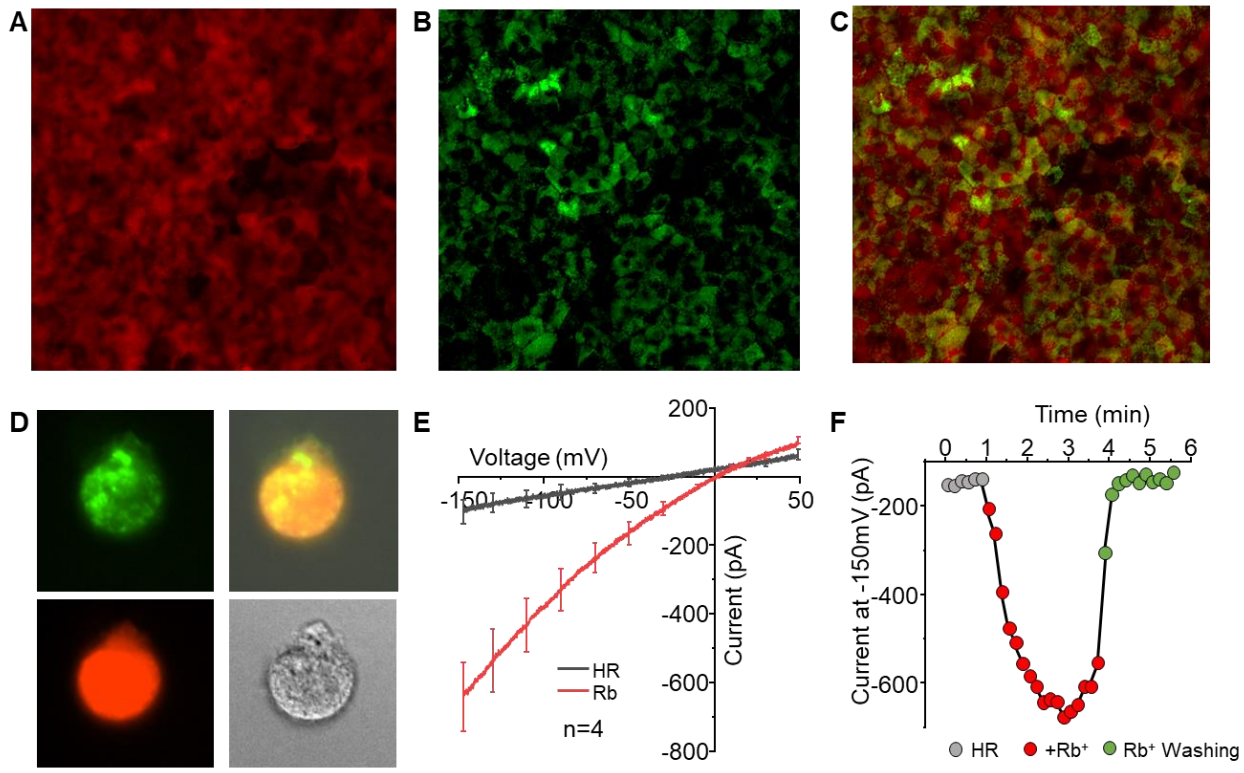

Figure 1: CRISPR-Cas9 gene editing outcomes in iPSC RPE^{W53X} cells. *A] Transduction of iPS-RPE cells with LentiCRISPRv2 –mCherry carrying sgRNA. B] Delivery of ssODN-ATTO 448 via silica nanoparticle. C] Merged image with fluorescence from both reporters. D] Dissociated RPE single-cell with a dual reporter following transduction and ssODN-488 delivery chosen for manual patch-clamping. E] Patch-clamp recording from the edited cell showing functional recovery of the Kir7.1 channel. F] Time course measurement showing the current increment with Rb+ and subsequent restoration of physiological K^+ current after washing.*

2. Validation of ABEs in HEK^{W53X}cell line confirms the activity and specificity of ABE8e-NG mRNA

As the HDR-mediated CRISPR-Cas9 gene editing showed lower efficiency in iPSC-RPE^{W53X} cells, we used CRISPR BE to correct W53X mutation. To quickly validate the potential ABEs along with human *KCNJ13* specific sgRNA for W53X editing with functional analysis in vitro, we generated HEK293 FRT W53X stable cells, hereby referred to as the HEK^{W53X} cell line. The construct design for creating the stable cells is shown in Fig 1A. These cells were genotyped to confirm the stable integration of a GFP-tagged *KCNJ13* gene [Fig 1B]. WT stable cells (HEK^{WT}) were created alongside Kir7.1 channel expression and functions for comparison. To develop a base editing strategy capable of correcting LCA16 mutation (*KCNJ13*, c.158G>A), specific sgRNAs were designed using Benchling and also validated with two other online tools, CRISPR-RGEN[30] and PnB Designer[31], to confirm its on-target specificity (Supplementary Table 7). Only

one sgRNA [Fig 1C] appeared to be very specific for the W53X location (GCGCTaGCGTTGGATGATGT, PAM; TGG) as it would allow the binding of the spCas9 domain to the target locus that positions c.158G>A site within the editing window of ABE (4-8 for ABE8e, counting the PAM as 21-23). We tested the activity of ABE8e-NG BE in mRNA and protein forms. HEK^{W53X} cells were electroporated with ABE8e-NG mRNA along with sgRNA (3:1 molar ratio) or with RNP complexes prepared by incubating ABE8e protein with sgRNA for 10 mins. Deep sequencing analysis on the pool of electroporated HEK^{W53X} cells showed significantly higher AT to GC correction efficiency with ABE8e mRNA (50.29 ± 1.38%) compared to ABE8e RNP (31.44 ± 3.39%) [Fig 1D]. Our on-target indel analysis showed minimal activity at and around the protospacer, comparatively higher in ABE8e mRNA treated cells than ABE8e RNP treated ones [Fig 1E].

The W53X nonsense mutation in *KCNJ13* disrupts its protein expression in HEK^{W53X} cells and successful editing of W53X was demonstrated by the restoration of Kir7.1 expression. Our immunocytochemistry analysis using GFP antibody showed that Kir7.1 protein is expressed in the membrane in most of the HEK$^{W53X\text{-}BE}$ cells, like control HEK^{WT} cells while in the HEK^{W53X}, it is accumulated in the nucleus due to its premature truncation [Fig 1F]. These results confirmed the successful translation and trafficking of full-length protein after the editing which is likely to be functional [Fig 1F]. Untreated HEK^{W53X} stable cells were used as reference.

To test the Kir7.1 channel function, whole-cell currents were recorded from the pool of HEK$^{W53X\text{-}BE}$ cells using an automated patch-clamp system. HEK^{WT} cells were used as positive control, and untreated HEK^{W53X} cells were used as a reference [Fig 2A-C]. In a standard external physiological Ringer's solution, HEK^{WT} cells had a large negative membrane potential (-74.24 ± 4.16 mV, n=3) (Supplementary Figure 4a) and exhibited an inward rectifying average Kir7.1 current of -19.6 ± 4.15 pA (n=26) at -150 mV in 5 mM K^+. The inward current was activated in HEK^{WT} cells in response to external 140 mM Rb^+ by 7.5-fold (-146.65 ± 30.13 pA), which is the characteristic of Kir7.1 current. However, the current did not get blocked by the addition of 20 mM Cs^+ to bath solution (-19.0 ± 3.58 pA), suggesting a low Cs^+ sensitivity of Kir7.1 channel [Fig 2A]. These responses were not observed in HEK^{W53X} untreated cells [Fig 2B]. These mutant cells

showed significantly lower current amplitude (-9.71 ± 1.26 pA) compared to HEK^{WT} cells with negligible response to external Rb^+ (-19.35 ± 2.50 pA) and Cs^+ (-9.58 ± 1.67 pA). On the other hand, $HEK^{W53X\text{-}BE}$ cells showed the characteristic K^+ current because of full-length Kir7.1 protein production in 80% of the cells (n=60) edited by ABE8e mRNA [Fig 2C]. These cells showed K^+ conductance of -33.33 ± 7.68 pA which was increased by 11-fold in external Rb^+ (-415.22 ± 54.0 pA) while Cs+ sensitive component was low (-42.19 ± 9.56 pA). The K^+ current profile of 20% of the $HEK^{W53X\text{-}BE}$ cells (n=15) was comparable to HEK^{W53X} untreated cells, which were most likely the unedited cells (K^+ current in Ringer's; -30.92 ± 8.04 pA, Rb^+; -57.67 ± 12.46 pA, Cs^+; -13.89 ± 5.07 pA) [Fig 2C]. The fold changes for Rb^+ and Cs^+ among different cell types are shown in Supplementary Figure 4b. The current-sweep plots for a representative cell type in different solutions are shown in Fig 2A-C. Overall, these results in $HEK^{W53X\text{-}BE}$ cells indicated that the on-target DNA editing activity of ABE8e mRNA to convert W53X>WT was remarkably higher compared to ABE8e RNP and it also resulted in a functional Kir7.1 channel.

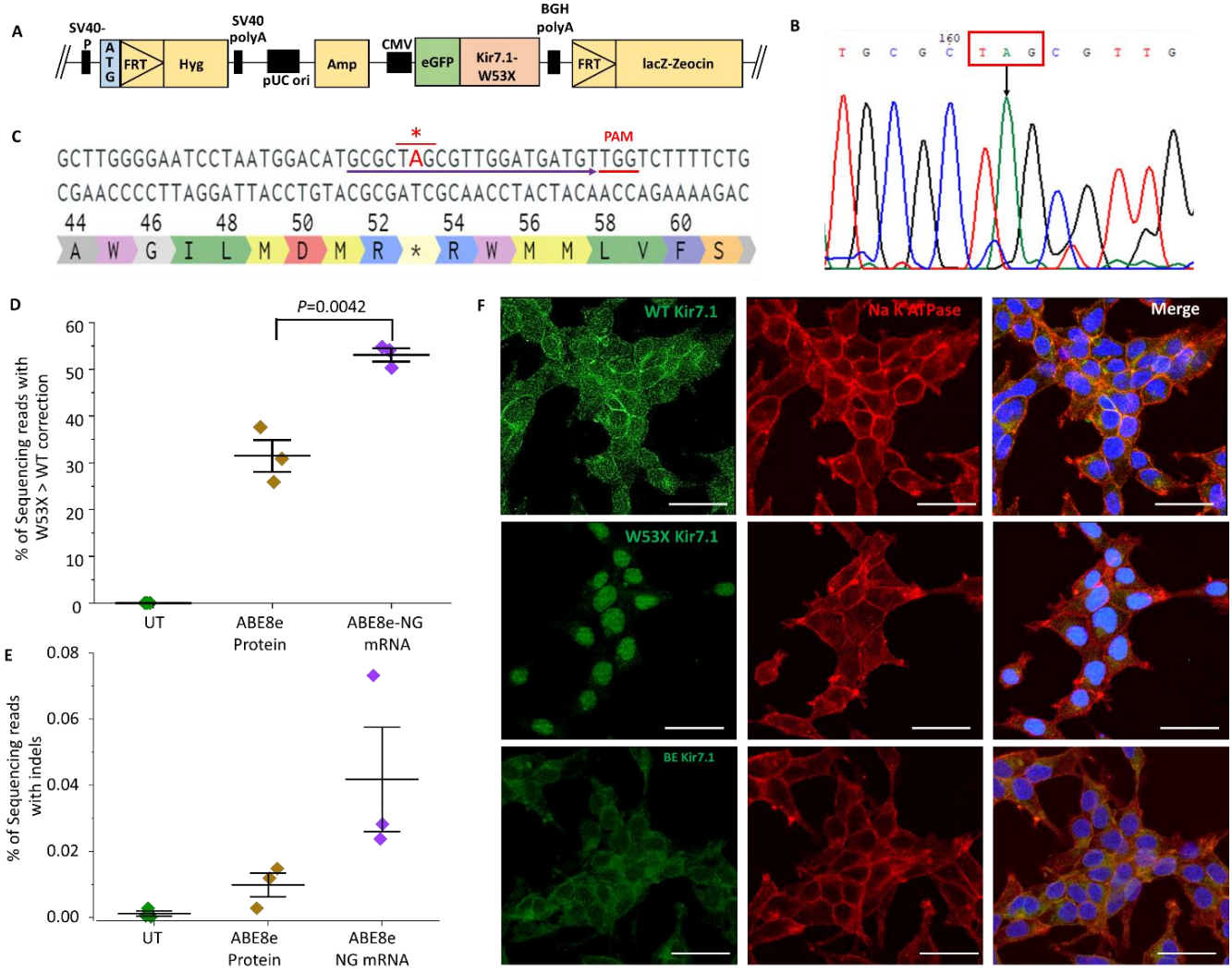

Figure 2: Evaluation of CRISPR ABE8e RNP and ABE8e-NG mRNA to correct hKCNJ13$^{W53X/W53X}$ allele in HEK293 FRT stable cells. *A] Construct design to create HEK293 FRT stable cells. B] Schematic of hKCNJ13 locus highlighting the mutation c.158G>A (in red marked with *) and position of W53X targeting specific sgRNA with TGG PAM (underlined in red). C] Chromatogram generated from HEK293 FRT stable cells showing the W53X codon marked in the red box and the downward black arrow showing the specific nucleotide change (G>A). D] Base editing efficiencies via electroporation showing the W53X>WT correction with no other silent changes, bystander edits, or indels in ABE8e RNP and ABE8e-NG mRNA treated stable cells (n=3). E] % of sequencing reads in with indels in ABE8e RNP and ABE8e-NG mRNA treated stable cells (n=3). F] Kir7.1 expression in BE ABE8e mRNA treated cells assessed by immunocytochemistry. Markers (diamonds) represent the individual biological replicates (n=3), and error bars represent SEM.*

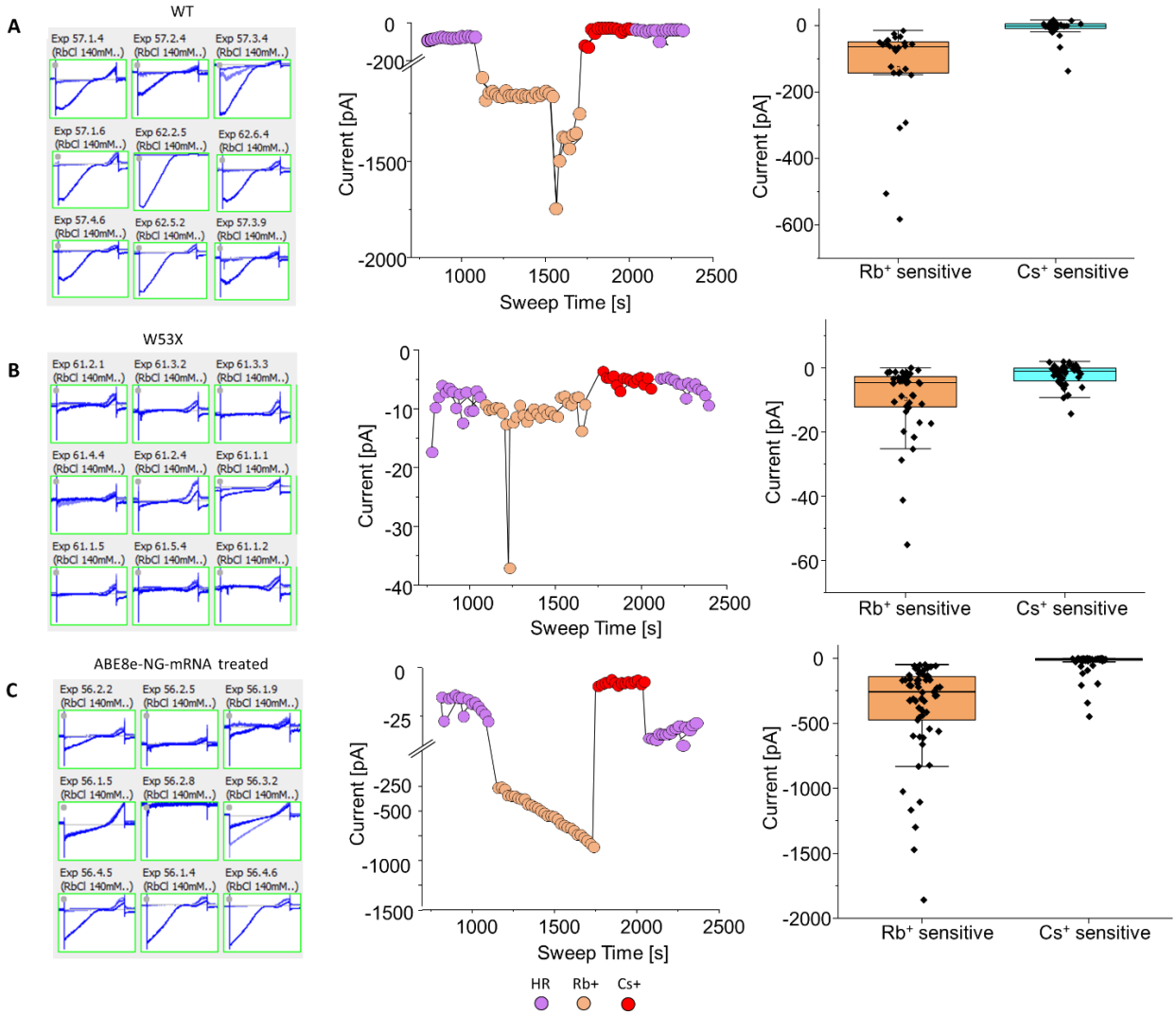

Figure 3: Kir7.1 current profile generated on an automated patch clamp system in WT, W53X and base edited W53X HEK293 FRT stable cells. *A] Snapshot of Kir7.1 current profile in WT stable cells. Current-Sweep plot is shown for one representative cell. Rb^+ and Cs^+ sensitive current in HEK^{WT} stable cells B] Snapshot of Kir7.1 current profile in HEK^{W53X} stable cells. Current-Sweep plot is shown for one representative cell. Rb^+ and Cs+ sensitive current in HEK^{W53X} stable cells. C] Snapshot of Kir7.1 current profile in $HEK^{W53X\text{-}BE}$ cells using ABE8e mRNA. Current-Sweep plot is shown for one representative cell. Rb^+ and Cs+ sensitive current in $HEK^{W53\text{-}BE}$cells.*

3. **Ex vivo base editing in patient's specific fibroblasts using ABEs encapsulated SNPs showed high efficiency.**

Ex vivo base editing could be a treatment option in patients with advanced LCA16 where the retina begins to deteriorate. As these patients lack healthy retinal cells for correcting the gene function in vivo, the fibroblasts from these patients can be base-edited, ex vivo and programmed and differentiated to mature RPE for the autologous transplantation and cell therapy to exert therapeutic effect which can partially restore the Kir7.1 channel function. Our base editing in HEK^{W53X} cells via electroporation showed higher

editing efficiency using mRNA than RNP. Therefore, the mRNAs approach was further used to edit the W53X mutation in LCA16-W53X-Patient's specific fibroblasts (Fibro^{W53X}). We used two different ABE mRNAs (ABE8e-NG, editing window 4-8 nt bases, and ABEmax, editing window 4-7 nt bases, counting PAM as 21-23) encapsulated SNPs to edit the W53X site as these ABEs have the same PAM recognition and share the similar editing window. Both the ABEs and the sgRNA were delivered to FibroW53X cells by SNP-PEG. Their editing efficiency, on-target substitutions, indels and bystander edits were compared 5 days post-treatment by deep sequencing. The SNP-PEGs used in this study (Fig 4A) were evaluated earlier for their efficiency and biocompatibility with different biomolecules like RNPs, mRNA, and plasmid DNA[24]. As expected, the editing efficiency of ABE8e-NG (52.31 ± 0.06%) to induce 'AT' to 'GC' conversion at the target W53X site (A^{6}) was significantly higher than (*p* value= 0.000027) than ABEmax (14.93 ± 1.73%). Both the treated cell types showed a few of the reads which were incorrectly edited (ABE8e; 6.48 ± 1.44%, ABEmax 4.67 ± 0.79%), and a few of them also had indel formations (ABE8e; 2.71 ± 0.40%, ABEmax; 1.35 ± 0.42%) [Fig 4B]. Our on-target analysis to assess the editing at other bystanders 'A's within the protospacer showed fewer A>G conversion in ABEmax treated cells (A^{14}; 0.09 ± 0.09) compared to ABE8e (A^{14}; 0.26 ± 0.03%, A^{17}; 0.07 ± 0.07%) [Fig 4C]. We also observed some ABE activity outside the protospacer, more specifically downstream of the protospacer region (A^{-2}, A^{-4}, A^{-8}, A^{-9}). ABEmax showed A>G transition at A^{-2} (0.07 ± 0.07%) and A^{-4} (0.15 ±0.08%) at very low frequency. ABE8e has comparatively a wider span of editing and exhibited A>G transition at A^{-9} (0.08 ± 0.08%) site along with A^{-2} (0.34 ± 0.025%) site [Fig 4C]. This bystander, 'A' editing within and outside the protospacer, resulted in silent (L48L) and missense mutations (D50G, M51V, M56V, M57V). These mutations were observed at a very low frequency (<1%) in Fibro^{W53X} [Fig 4D] and possibly may not affect the protein function when programmed and differentiated to mature RPE. Untreated Fibro^{W53X} cells were used as reference (Supplementary Figure 5). Fig 4E and 4F show the top 10 reads with mutation, on-target editing, indels, and other substitutions generated by ABEmax and ABE8e treatment, the frequency of which was <0.5%. These results confirmed the on-target specificity of two BEs and the higher activity of ABE8e at the W53X site.

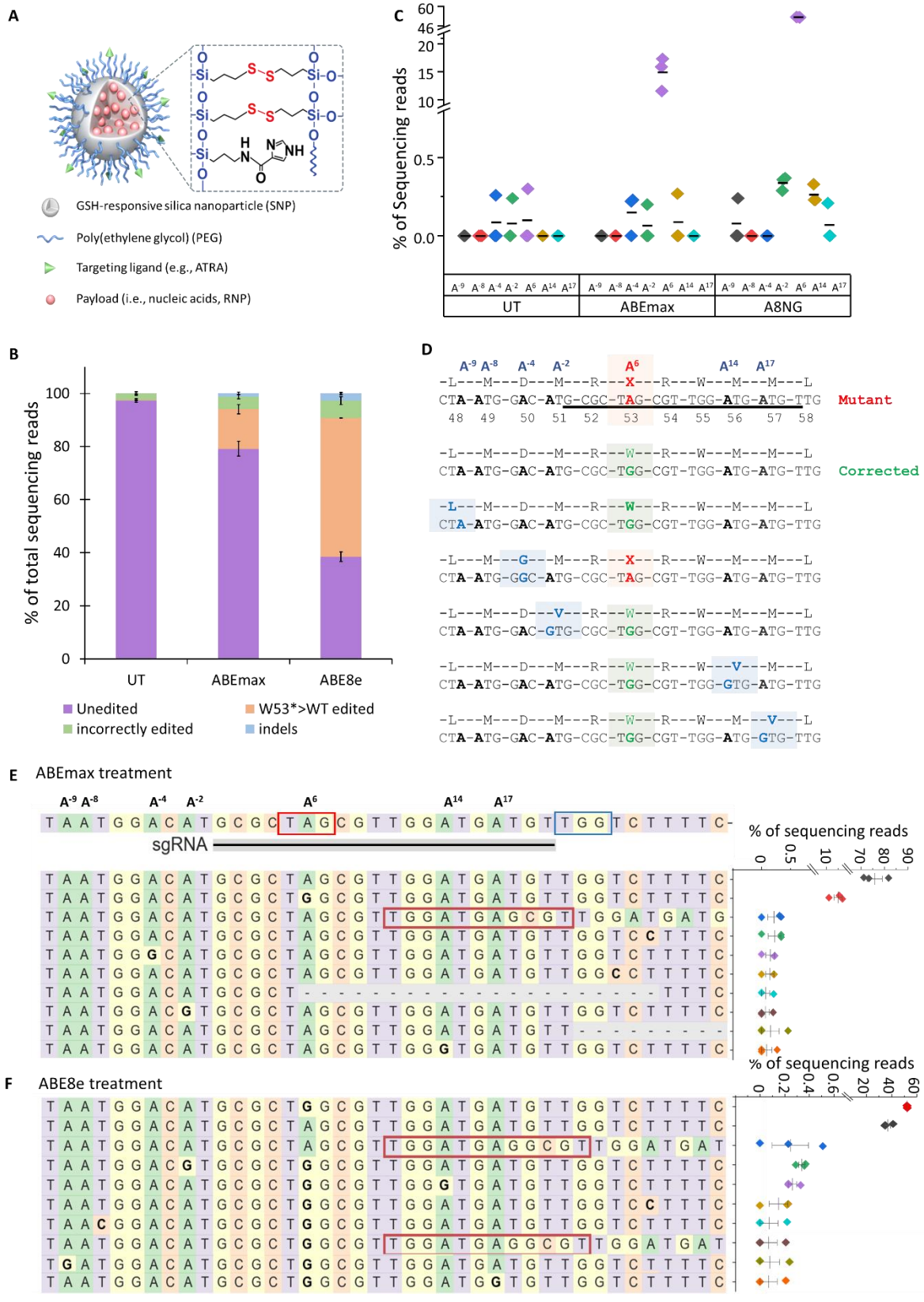

Figure 4: Evaluation of two CRISPR ABE mRNAs and guide RNA combinations to correct W53X allele in LCA16-patient's specific fibroblasts. *A] Design of Silica nanoparticles[24], used to encapsulate BE mRNA and sgRNA. B] Base editing efficiencies depicting the % of total DNA sequencing reads, classified as unedited, correctly edited, incorrectly edited, and with indels in treated and untreated cells. C] % Editing of the target (A^{6}) and bystander (A^{-9}, - A^{-8}, A^{-4}, A^{-2}, A^{14}, A^{17}) 'A' to 'G' by ABEmax and ABE8e mRNA as observed in three independent experiments. D] Amino acid conversion at the respective location generated due to target and bystander A edits. The location of sgRNA is underlined, the mutation is depicted in red/bold, target 'A' edit is marked in green, and bystander 'A' edits in blue. E] The sgRNA location is underlined, PAM is marked in the blue box, and mutation in the red box. All the 'A' bases within the protospacer are numbered from 1-20 based on their location. The 'A' bases downstream of the protospacer are numbered from -1 to -9, considering +1 as the first base of the protospacer. Top 10 reads generated by ABEmax mRNA treatment showing the nucleotide distribution around the cleavage site for sgRNA. Substitutions are highlighted in bold, insertions are shown in the red box, and deletions are shown by a dashed line '-'. The scatter plot shows the frequency of reads observed in treated cells (n=3). F] Top 10 reads generated by ABE8e-NG mRNA treatment showing the nucleotide distribution around the cleavage site for sgRNA. Substitutions are highlighted in bold, insertions are shown in the red box, and deletions are shown by a dashed line '-'. The scatter plot shows the frequency of reads observed in treated cells (n=3). Figures presenting pooled data are represented as mean ± SEM.*

4. **Successful editing in patients-derived iPSC RPE showed restoration of Kir7.1 channel function.**

Next, we tested the base editing efficiency in iPSC RPE^{W53X} using ABE8e as it showed better on-target activity in Fibro^{W53X}. ABE8e-NG mRNA and sgRNA were encapsulated in SNP-PEG and delivered to the cells. SNP-PEG particles have been beneficial in delivering CRISPR tools to RPE, as transfecting the RPE by standard means or uncovering engineered AAV-serotypes that can transduce RPE have been a challenge. In addition, to other pitfalls of these techniques. We did not observe any noticeable toxicity in the ABE8e treated RPE, and its morphology was comparable to untreated iPSC RPE^{W53X} [Fig 5A]. Deep sequencing analysis in the iPSC RPE$^{W53X\text{-}BE}$ demonstrated high on-target specificity but relatively low efficiency (17.82 ± 1.53%) of ABE8e [Fig 5B]. Surprisingly, the other reads with indels (0.68 ± 0.11%) and substitutions (2.94 ± 0.42%) were above the baseline as observed in untreated iPSC RPE^{W53X} cells (indels; 0.01 ± 0.002%, substitutions; 1.78 ± 0.07%) (Supplementary Figure 6) but the frequency was very low [Fig 5C].

A manual patch-clamp was carried out on the pool of iPSC RPE$^{W53X\text{-}BE}$ cells [Fig 5D] to confirm the functional rescue of the Kir7.1 channel. Cells were picked up randomly as no reporter gene or a selection marker was present to identify the edited cells. Three different kinds of Kir7.1 current profiles were observed in the iPSC RPE$^{W53X\text{-}BE}$ pool. Some of the cells (n=5) showed a reasonable amplitude of K+

conductance (-101.98 ± 0.07 pA) in Ringer's solution, which was potentiated in Rb^+ external solution by 8-fold (-820.97 ± 265.54 pA). These were the high responding cells in the pool that showed rescue of Kir7.1 channel function and most liked have only W53X>WT correction. Some of the cells did not show any rescue of Kir7.1 current (Ringer's; -33.66 ± 31.59 pA, Rb^+; -80.51 ± 19.37 pA) and had a similar profile as iPSC RPE^{W53X} cells[12]. These were the low responding single cell (n=4) which might not have W53X>WT correction in any of the alleles. A few cells showed slightly higher Rb^+ current than the untreated iPSC RPE^{W53X} cells, but not like iPSC RPE^{WT} cells. These were the medium responding cells that showed only a 3-fold Rb^+ response (-238.74 ± 102.13 pA) for the current amplitude observed in Ringer's solution (-72.57 ± 29.74 pA). The current-sweep plots of the representative cell under different treatment solutions are shown in Fig 5E.

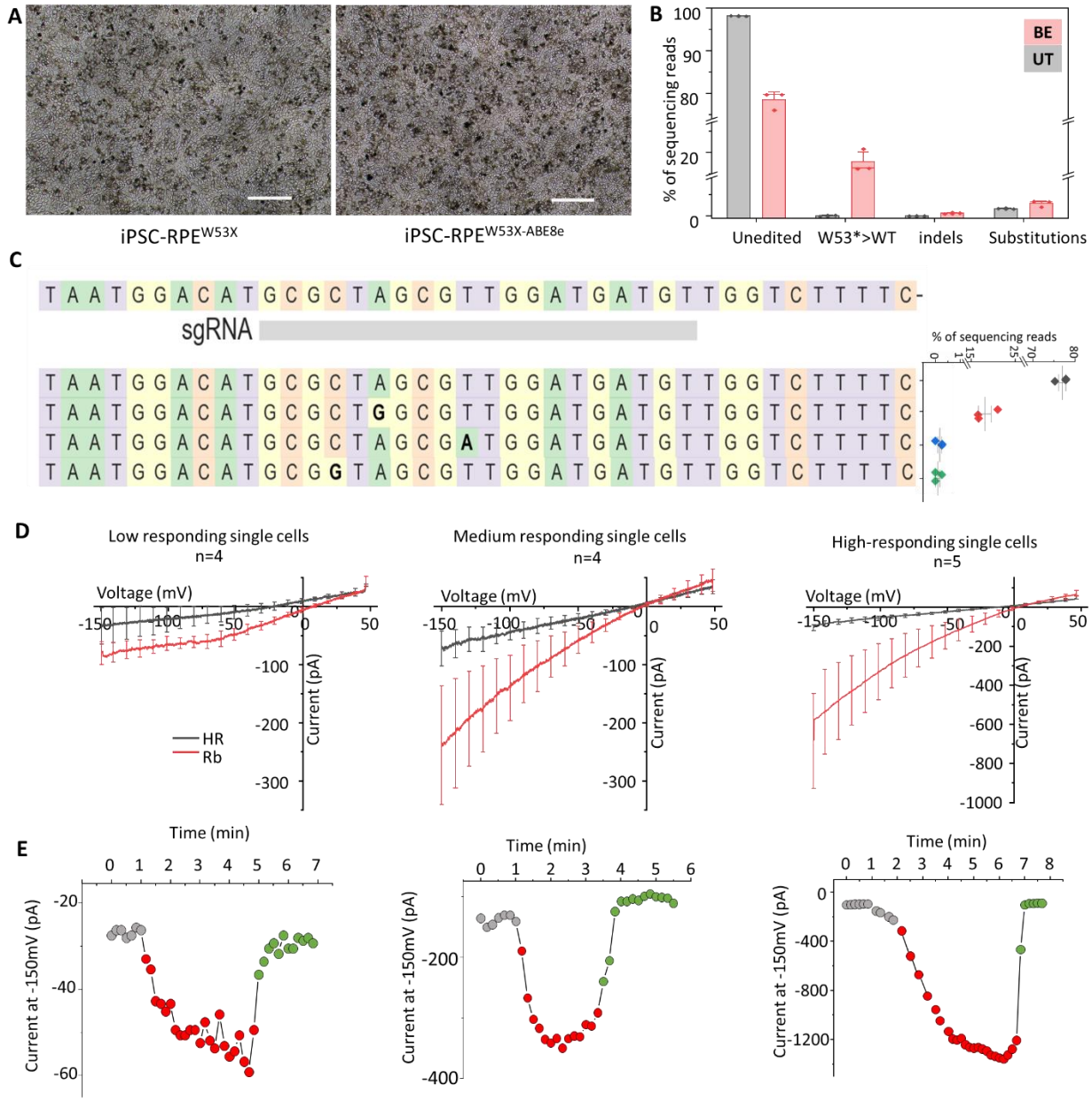

Figure 5: Evaluation of ABE8e to correct W53X allele in iPSC RPE^{W53X}. *A] Representative bright-field images of BE treated and untreated iPSC RPE^{W53X}. B] Base editing efficiencies for the ABE8e mRNA and sgRNA encapsulated SNP-PEG C] Reads generated by ABE8e-NG mRNA treatment showing the nucleotide distribution around the cleavage site for sgRNA. Substitutions are highlighted in bold. The scatter plot shows the frequency of reads observed in treated cells (n=3). Figures presenting pooled data are represented as mean ± SEM. D] Manual single-cell patch-clamp assay from the pool of iPSC RPE$^{W53X\text{-}ABE8e}$ edited cells showing three different responses. Low responding single cells, which appeared to be mutant, medium responding single cells, which showed a low level of Rb^+ response, and high responding single cells, which showed Rb^+ response like iPSC RPE^{WT} cells. E] Current-sweep plot from a representative cell of each type showing the different solution treatment (physiological Ringer solution; gray, Rb^+; red, wash with Ringer; green). Figures presenting pooled data are represented as mean ± SEM.*

5. In vivo base editing partially rescues Kir7.1 functions and ERG phenotype in LCA16$^{W53X/-}$ mice.

A major limitation to validating the in vitro finding of *KCNJ1*^{3W53X} correction is the unavailability of in vivo mouse model with biallelic homozygous mutants. Unlike LCA16 patients, *Kcnj13* in mice has shown the survival need and demands at least one normal allele of this gene[32]. As homozygous W53X mice (*Kcnj13*$^{W53X/W53X}$) do not survive, we took advantage of our heterozygous mice (*Kcnj13*$^{W53X/+}$) and disrupted the WT *Kcnj13* allele only in RPE using CRISPR/Cas9 RNPs encapsulated SNP-PEG-ATRA, delivered via subretinal injections. A full field scotopic ERG was performed on *Kcnj13*$^{W53X/+}$ mice before the disruption to assess the normal visual function. The amplitude of the a-wave, b-wave, and c-wave of the scotopic ERG for these mice were 157.76 ± 20 µV, 380.9 ± 57.3 µV at 10 cd.s/m^{2,} and 350.93 ± 31.16 µV at 25 cd.s/m^2 respectively. The *Kcnj13*$^{W53X/+}$ mice with normal visual functions were used to create the LCA16 phenotype by disrupting the WT allele. Two weeks following injection of RNPs, a decrease in a-wave (59.74 ± 4.73 µV), b-wave (137 ± 5 µV), and c-wave (110.7 ± 41.7 µV) were observed. The a-wave and b-wave recovered somewhat after 4 and 6 weeks, but the c-wave, which originates from RPE cells, had an almost 70 % reduction in amplitude in all follow-up ERGs. These mice, with the reduced or loss of ERG c-wave, were then used as an LCA16 model (*Kcnj13*$^{W53X/-}$) to validate our in vitro findings. All the sgRNAs targeting either the WT or W53X allele of mouse *Kncj13* were designed using the Benchling online tool and validated in in vitro mouse fibroblasts (Supplementary Table 8, Supplementary Figure 7).

For correcting the single W53X allele in *Kcnj13*$^{W53X/-}$ mice, ABE8e mRNA and sgRNA targeting the W53X allele and GFP mRNA were packaged into SNP-PEG-ATRA (100 pmol) and delivered via subretinal injections. GFP mRNA (1 µg) was used in the complex to locate the injection site. We used two doses of ABE8e mRNA (2 µg and 3 µg) to establish its potential and editing efficiencies. For deep sequencing analysis, GFP positive murine RPE area was cut to isolate the g.DNA and W53X-*Kncj13* site was amplified. We observed higher editing efficiency (9.48 ± 3.26%) using 3 µg of ABE8e (n=4 eyes), while a lower dose of 2 µg (n=4 eyes) showed lower editing efficiency (4.73 ± 2.51%) to correct W53X>WT in *Kcnj13*$^{W53X/-}$ mice. Our on-target analysis showed no other A>G substitutions outside or within the protospacer region,

but indels mutations (2 μg; 0.04 ± 0.002%, 3 μg; 0.04 ± 0.0007%) were observed at a very low frequency, similar to placebo (PBS/ empty SNP-PEG-ATRA; 0.03 ± 0.01%) treated mice.

The *Kcnj13*$^{W53X/-}$ base edited mice were subjected to ERG to confirm the functional outcomes of editing. These mice (n=3 eyes) underwent ERG monitoring at 2, 4, 8, and 12 weeks. In the 2nd week following the injection, the amplitude of a-, b-, and c- waves was reduced, but by the 6th week, the amplitude of c- waves had returned to the level observed after the disruption of the WT allele. At week 8, a slight increase in the amplitude of the c-wave was noticed with an amplitude of 137.57 ± 60.14 μV, which was followed by a further increase at week 12 and week 20 by 139.85 ± 22 and 153.22 ± 75.12, respectively. These data demonstrate the phenotypic reversal of mutant RPE following base editing by ABE8e encapsulated SNP-PEG-ATRA.

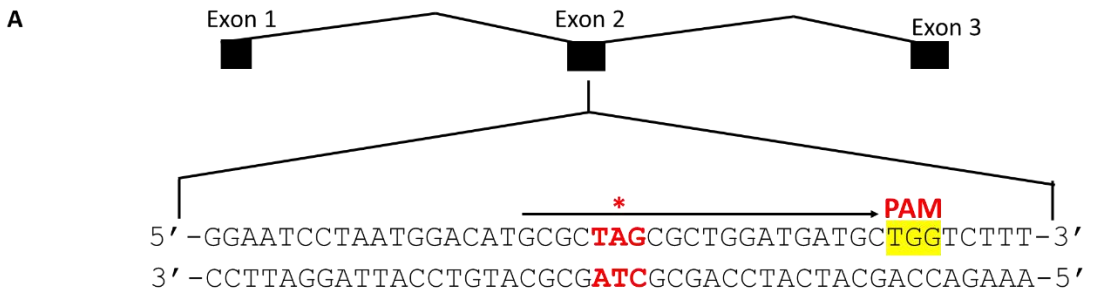

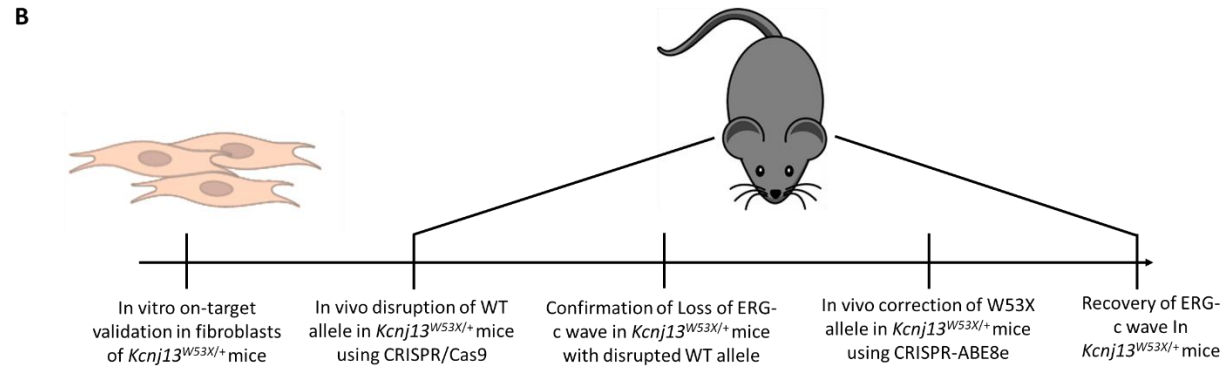

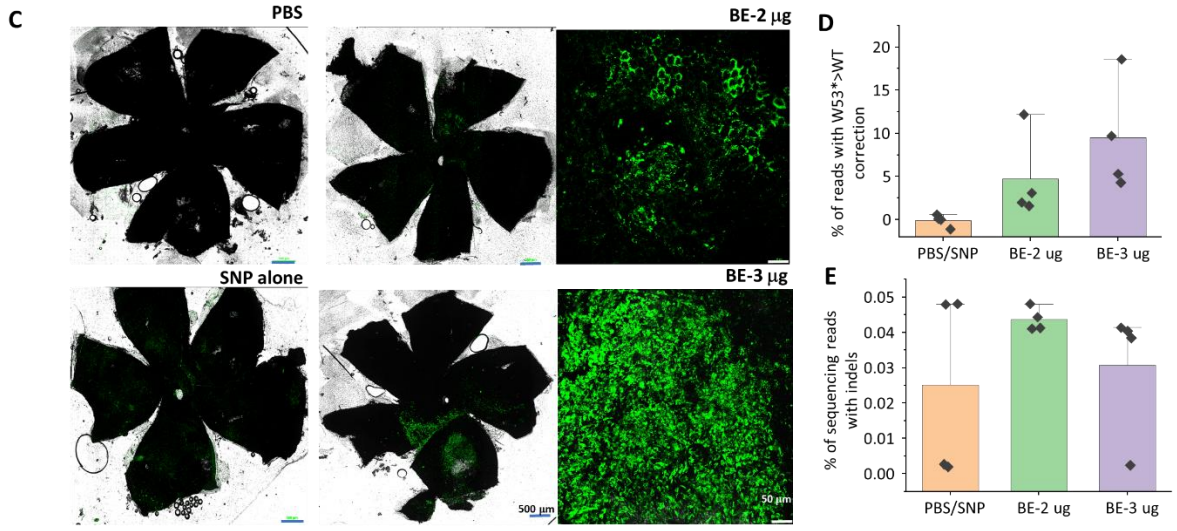

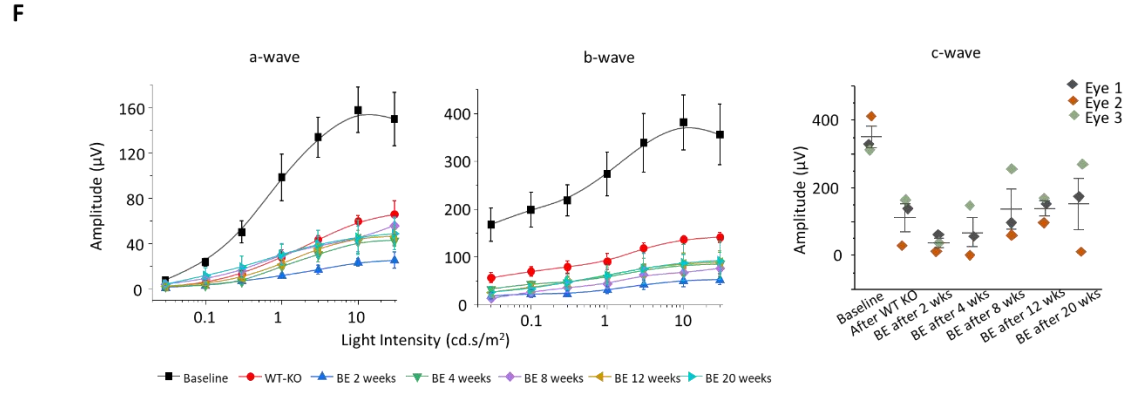

Figure 6: Phenotypic reversal of mutant RPE following ABE8e and sgRNA encapsulating SNP-PEG-ATRA. *A] The sgRNA design targeting the Kcnj13^{W53X} allele for base editing was designed using Benchling. B] Workflow of in vivo base editing strategy. C] RPE floret of eyes subretinally injected with SNP-PEG-ATRA packaged ABE8e mRNA, W53X-sgRNA, and GFP mRNA or empty SNP-PEG-ATRA/PBS used as placebo. D] % of sequencing reads showing the W53X>WT corrections, observed in Kcnj13$^{W53X/-}$ mice treated with 2 μg or 3 μg of ABE8e. E] % of sequencing reads showing the indels, observed in Kcnj13$^{W53X/-}$ mice treated with 2 μg or 3 μg of ABE8e. F] ERG responses to 10 cd.s/m2 flash stimuli recorded under dark-adapted conditions in ABE8e treated Kcnj13$^{W53X/-}$ mice (n=3 eyes) showing a-, b- and c-wave amplitudes from the retina before (black line) and after the WT disruption (red line) and at 2, 4, 8, 12, and 20 weeks following base editing. The c-wave amplitude was recorded at 25 cd.s/m2 following disruption of the WT allele and base editor correction of the mutant allele. Figures presenting pooled data are represented as mean ± SEM.*

6. Off target analysis of sgRNA for human and murine W53X target confirms the target specificity

CRISPR-based BEs may enable simultaneous targeting of multiple DNA sites leading to robust gene modification across the genome due to partial match with sgRNA sequence. Therefore, it is essential to screen some of the potential sites to confirm the target specificity. We used an online computational algorithm, Cas-OFFinder[33], to identify the putative off-target sites for W53X-sgRNA. We considered up to maximum of 4 mismatches to sgRNA sequence with or without a DNA-bulge of 1 nucleotide, which occurs due to an extra unpaired base in the DNA sequence with respect to sgRNA or RNA bulge of 1 nucleotide, which occurs due to an extra unpaired base in sgRNA sequence with respect to the DNA sequence in the genome. The likelihood of off-target effects is more at the sites with 1-2 mismatches with no DNA/RNA bulge, but our in-silico analysis showed no such off-target sites for this sgRNA. We found 2727 off-target sites to W53X-sgRNA, of which most of the sites harbored 4 mismatches with 1 nucleotide RNA bulge (n=2004) or DNA bulge (n=512). 141 off-target sites were with 3 mismatches/ 1 RNA bulge, 31 with 4 mismatches/ no bulge, and 27 with 3 mismatches/ 1 DNA bulge. All other combinations of mismatches and DNA/RNA bulge showed very few off-target sites (n<10), which are likely to be edited by ABE8e (Supplementary Figure 2).

We analyzed the off-target activity of ABE8e in HEK$^{W53X\text{-}BE}$, LCA$^{W53X\text{-}BE}$, and iPSC RPE$^{W53X\text{-}BE}$ cells at the top nine potential sites (Supplementary Table 4). The untreated cells, HEK^{W53X}, LCA^{W53X}, and iPSC RPE^{W53X} were used as references. Deep sequencing analysis of these sites showed that ABE8e had minimal off-target activity in terms of AT to GC substitution (<0.02%) and indel formation (<0.006%), which was comparable to baseline substitutions and indels observed in reference cells [Fig 7A,7B]. These data

demonstrate that the off-target modification levels of ABE8e at every nine potential sites are much lower than its on-target editing efficiency. Our results also indicated that DNA/ RNA bulges at these off-target sites were well tolerated and did not result in any substitutions/indels.

For the detection of in vivo off-target effect of ABE8e and mouse sgRNA targeting the W53X allele, we used rhAMP PCR technique to screen all the 11 potential sites (Supplementary Table 6) in one sequencing run, which Cas-OFFinder identified. For this, the g.DNA sample was used from the optic cup of the treated heterozygous mice without any WT disruption (*Kcnj13*$^{W53X/+}$), which showed on-target W53X>WT correction. We observed similar results as in our in vitro experiments. The frequency of sequencing reads with indels and NHEJ was <0.4% in these mice [Fig 7C, 7D]. Our results confirmed that for the applications like therapy development and disease treatment, where the off-target mutations must be kept at a minimal, ABE8e could be one of the potential BEs for AT to GC gene correction.

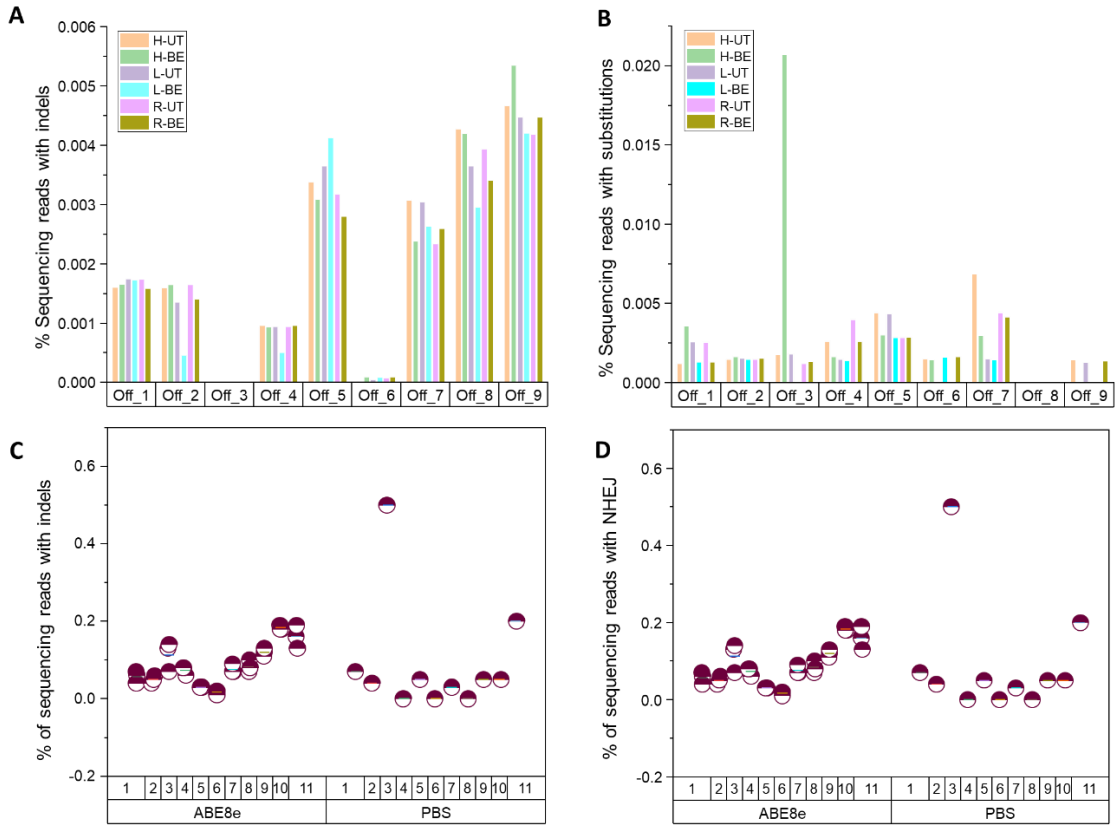

Figure 7: Deep sequencing analysis at putative off-target sites in in vitro and in vivo ABE8e edited samples. *A] in vitro; % of sequencing reads with indels as observed in deep sequencing analysis in HEK*^{W53X}*, Fibro*^{W53X,} *and iPSC RPE*^{W53X} *and their respective untreated cells. B] in vitro; % of sequencing*

reads with substitutions as observed in deep sequencing analysis in HEK^{W53X}, Fibro^{W53X,} and iPSC RPE^{W53X} and their respective untreated cells. C] in vivo; % of sequencing reads with indels as observed in deep sequencing analysis in ABE8e treated Kcnj13$^{W53X/+}$ (n=3 eyes) with respect to PBS treated Kcnj13$^{W53X/+}$mouse (n=1 eye). D] in vivo; % of sequencing reads with NHEJ as observed in deep sequencing analysis in ABE8e treated Kcnj13$^{W53X/+}$ (n=3 eyes) with respect to PBS treated Kcnj13$^{W53X/+}$mouse (n=1 eye). Figures presenting pooled data are represented as mean ± SEM.

Discussions

Until now, recessive loss-of-function *KCNJ13* point mutations are the only known genetic cause of LCA16, which disrupt the Kir7.1 channel function and alter the RPE physiology, leading to retinal degeneration with progressive vision loss in patients. Correcting these mutations in the genome could permanently restore the Kir7.1 channel function and revert the disease phenotype. Of the 12 different LCA16-causing mutations (as reported in HGMD® Professional 2022.1)[34], base editors can correct 8 mutations and 5/8 can be corrected using ABE requiring A>G (or T>C) corrections[29]. This study focused on W53X mutation to determine the functional rescue of correcting a single base change (A>G) using ABEs in vitro and in vivo LCA16 models. Our HEK293 stable cells have been a very useful tool to quickly validate the base editing outcomes, protein expression, and functions in edited cells[29]. A >50% editing efficiency in HEK$^{W53X\text{-}BE}$ via electroporation indicated 50-100% of the cells being edited based on monoallelic or biallelic corrections. K+ conductance in the HEK$^{W53X\text{-}BE}$ cells confirmed the rescue of Kir7.1 channel function upon ABE8e mediated base editing, which is possible only when the channel is able to assemble into its tetrameric structure and get trafficked to the membrane.

We packaged the ABE8e into SNP-PEG to edit the Fibro^{W53X} cells ex vivo. We observed similar editing efficiency in our Fibro^{W53X} cells (>50%), suggesting that SNP-PEG formulation is an appropriate alternative depot to deliver the BEs/sgRNA. This approach is particularly valuable in patients who have already started or at the verge of RPE degeneration due to a prolonged diseased state in the absence of any treatment and no more have healthy RPE for in vivo base editing. The ex vivo edited RPE can be used as cell therapy in these patients. Another advantage of ex vivo base editing is we can filter the cells with any on-target indels and genome-wide off-targets. Although we did not observe any off-target activity of BE/sgRNA at the nine putative screened sites, unbiased off-target profiling of all the sites should be conducted before using these cells for transplantation purposes.

Our iPSC-RPE$^{W53X\text{-}BE}$ showed reduced editing efficiency (17.82%) when treated with ABE8e encapsulated SNP-PEGs. This could be due to the non-dividing nature of RPE, in which the DNA repair machinery is not as active as it is in the dividing cells. This could also account for variability in uptake properties of RPE

in a pool of edited cells. Despite lower correction efficiency, iPSC-RPE$^{W53X\text{-}BE}$ showed the functional rescue of the Kir7.1 channel. Moreover, like many other ocular diseases, LCA16 doesn't require the correction of all the mutant alleles in diseased cells. A fraction of mutant cell's correction is sufficient to revert the disease phenotype. Earlier, we showed that the pathological state of RPE can be reverted to normal by the rescue of 25% of the Kir7.1channel function[12]. Also, a recent Edit101 clinical trial on LCA10 causing *CEP290* gene confirmed the visual function in primates with >10% functional photoreceptors[21]. Altogether, these results demonstrated that the ABE8e's higher editing with no detectable off-target profile monopolizes its use over conventional Cas9-mediated gene editing, which showed only <8% efficiency in iPSC RPE^{W53X}.

Our study answers important questions about the efficacy of allele targeting and delivery of editing tools to murine RPE. In vivo delivery of ABE8e and sgRNA encapsulated SNP-PEG-ATRA via subretinal injection resulted in >10% editing efficiency in restoring the WT coding sequence in RPE cells of *Kcnj13*$^{W53X/-}$ mice, with minimal to no off-targets. We reasoned that the lower editing efficiency in *Kcnj13*$^{W53X/-}$ RPE could be due to our limitation in evaluating the activity of ABE8e against the single *Kcnj13*-W53X allele as homozygous mice with two *Kcnj13*-W53X alleles do not survive. The edited mice exhibited partial recovery of the ERG c-wave amplitudes with no further retinal degeneration, which supports the Kir7.1 functionality after the editing. Given that untreated mice have no detectable ERG c-wave as a function of vision, these base editing outcomes represent this study's important conclusion. For an LC16-patient with W53X mutation, a similar corresponding improvement would describe the difference between no visual function to being able to see at some level.

The other limitation of our study is that we have not done the clonal analysis of editing outcomes which is a critical aspect to look for when evaluating the multimeric Kir7.1 channel function. The tetrameric nature of the Kir7.1 channel makes the editing challenging at the cellular level. The stoichiometric ratio of an edited and unedited allele can change the fate of a cell and may negatively impact the protein functions. A clonal analysis would reveal if the allelic editing happened differently, resulting in function or no function in the cell[13].

In summary, although our study successfully restored some of the visual function in the W53X-mouse model of human LCA16, an improvement is required to increase the base editing efficiency by expanding the spread of SNP-mediated delivery of base editors in RPE. Nevertheless, these proof-of-concept data support the further development of base editing for correcting different *KCNJ13* point mutations with functional validation and its subsequent transition to clinical practice.

Acknowledgments
We thank the Stem Cell & Regenerative Medicine Center (SCRMC) fellowship for the funding support to Meha Kabra. We acknowledge Retina Research Foundation Kathryn and Latimer Murfee Chair, McPherson ERI (KS), MD. Matthews Research Professorship (BRP), NIH R01 EY024995 and R24 EY032434 (BRP). We acknowledge the present and past members of Pattnaik lab for their valuable input.

Competing interests
The authors declare that they have no competing interests.

References
1. Kumar M, Pattnaik BR. Focus on Kir7.1: physiology and channelopathy. *Channels (Austin)*. 2014;8(6):488-95. doi:10.4161/19336950.2014.959809
2. Kabra M, Pattnaik BR. Sensing through Non-Sensing Ocular Ion Channels. *Int J Mol Sci*. Sep 21 2020;21(18)doi:10.3390/ijms21186925
3. Toms M, Dubis AM, Lim WS, Webster AR, Gorin MB, Moosajee M. Missense variants in the conserved transmembrane M2 protein domain of KCNJ13 associated with retinovascular changes in humans and zebrafish. *Exp Eye Res*. Dec 2019;189:107852. doi:10.1016/j.exer.2019.107852
4. Sergouniotis PI, Davidson AE, Mackay DS, Li Z, Yang X, Plagnol V, Moore AT, Webster AR. Recessive mutations in KCNJ13, encoding an inwardly rectifying potassium channel subunit, cause leber congenital amaurosis. *Am J Hum Genet*. Jul 15 2011;89(1):183-90. doi:10.1016/j.ajhg.2011.06.002
5. Pattnaik BR, Tokarz S, Asuma MP, Schroeder T, Sharma A, Mitchell JC, Edwards AO, Pillers DA. Snowflake vitreoretinal degeneration (SVD) mutation R162W provides new insights into Kir7.1 ion channel structure and function. *PLoS One*. 2013;8(8):e71744. doi:10.1371/journal.pone.0071744
6. Hejtmancik JF, Jiao X, Li A, Sergeev YV, Ding X, Sharma AK, Chan CC, Medina I, Edwards AO. Mutations in KCNJ13 cause autosomal-dominant snowflake vitreoretinal degeneration. *Am J Hum Genet*. Jan 2008;82(1):174-80. doi:10.1016/j.ajhg.2007.08.002
7. Zhang W, Zhang X, Wang H, Sharma AK, Edwards AO, Hughes BA. Characterization of the R162W Kir7.1 mutation associated with snowflake vitreoretinopathy. *Am J Physiol Cell Physiol*. Mar 1 2013;304(5):C440-9. doi:10.1152/ajpcell.00363.2012
8. Carrington SJ, Hernandez CC, Swale DR, Aluko OA, Denton JS, Cone RD. G protein-coupled receptors differentially regulate glycosylation and activity of the inwardly rectifying potassium channel Kir7.1. *J Biol Chem*. Nov 16 2018;293(46):17739-17753. doi:10.1074/jbc.RA118.003238
9. Beverley KM, Shahi PK, Kabra M, Zhao Q, Heyrman J, Steffen J, Pattnaik BR. Kir7.1 disease mutant T153I within the inner pore affects K+ conduction. *Am J Physiol Cell Physiol*. May 18 2022;doi:10.1152/ajpcell.00093.2022
10. Pattnaik BR, Shahi PK, Marino MJ, Liu X, York N, Brar S, Chiang J, Pillers DA, Traboulsi EI. A Novel KCNJ13 Nonsense Mutation and Loss of Kir7.1 Channel Function Causes Leber Congenital Amaurosis (LCA16). *Hum Mutat*. Jul 2015;36(7):720-7. doi:10.1002/humu.22807

11. Shahi PK, Liu X, Aul B, Moyer A, Pattnaik A, Denton J, Pillers DM, Pattnaik BR. Abnormal Electroretinogram after Kir7.1 Channel Suppression Suggests Role in Retinal Electrophysiology. *Sci Rep*. Sep 6 2017;7(1):10651. doi:10.1038/s41598-017-11034-1
12. Shahi PK, Hermans D, Sinha D, Brar S, Moulton H, Stulo S, Borys KD, Capowski E, Pillers DM, Gamm DM, et al. Gene Augmentation and Readthrough Rescue Channelopathy in an iPSC-RPE Model of Congenital Blindness. *Am J Hum Genet*. Feb 7 2019;104(2):310-318. doi:10.1016/j.ajhg.2018.12.019
13. Steyer B, Bu Q, Cory E, Jiang K, Duong S, Sinha D, Steltzer S, Gamm D, Chang Q, Saha K. Scarless Genome Editing of Human Pluripotent Stem Cells via Transient Puromycin Selection. *Stem Cell Reports*. Feb 13 2018;10(2):642-654. doi:10.1016/j.stemcr.2017.12.004
14. Strong A, Musunuru K. Genome editing in cardiovascular diseases. *Nat Rev Cardiol*. Jan 2017;14(1):11-20. doi:10.1038/nrcardio.2016.139
15. Nami F, Basiri M, Satarian L, Curtiss C, Baharvand H, Verfaillie C. Strategies for In Vivo Genome Editing in Nondividing Cells. *Trends Biotechnol*. Aug 2018;36(8):770-786. doi:10.1016/j.tibtech.2018.03.004
16. Orthwein A, Noordermeer SM, Wilson MD, Landry S, Enchev RI, Sherker A, Munro M, Pinder J, Salsman J, Dellaire G, et al. A mechanism for the suppression of homologous recombination in G1 cells. *Nature*. Dec 17 2015;528(7582):422-6. doi:10.1038/nature16142
17. Gaudelli NM, Komor AC, Rees HA, Packer MS, Badran AH, Bryson DI, Liu DR. Programmable base editing of A*T to G*C in genomic DNA without DNA cleavage. *Nature*. Nov 23 2017;551(7681):464-471. doi:10.1038/nature24644
18. Hanlon KS, Kleinstiver BP, Garcia SP, Zaborowski MP, Volak A, Spirig SE, Muller A, Sousa AA, Tsai SQ, Bengtsson NE, et al. High levels of AAV vector integration into CRISPR-induced DNA breaks. *Nat Commun*. Sep 30 2019;10(1):4439. doi:10.1038/s41467-019-12449-2
19. Miller DG, Petek LM, Russell DW. Adeno-associated virus vectors integrate at chromosome breakage sites. *Nat Genet*. Jul 2004;36(7):767-73. doi:10.1038/ng1380
20. Nelson CE, Wu Y, Gemberling MP, Oliver ML, Waller MA, Bohning JD, Robinson-Hamm JN, Bulaklak K, Castellanos Rivera RM, Collier JH, et al. Long-term evaluation of AAV-CRISPR genome editing for Duchenne muscular dystrophy. *Nat Med*. Mar 2019;25(3):427-432. doi:10.1038/s41591-019-0344-3
21. Maeder ML, Stefanidakis M, Wilson CJ, Baral R, Barrera LA, Bounoutas GS, Bumcrot D, Chao H, Ciulla DM, DaSilva JA, et al. Development of a gene-editing approach to restore vision loss in Leber congenital amaurosis type 10. *Nat Med*. Feb 2019;25(2):229-233. doi:10.1038/s41591-018-0327-9
22. Fangueiro JF, Veiga F, Silva AM, Souto EB. Ocular Drug Delivery - New Strategies for Targeting Anterior and Posterior Segments of the Eye. *Curr Pharm Des*. 2016;22(9):1135-46. doi:10.2174/1381612822666151216145900
23. Kaur IP, Kakkar S. Nanotherapy for posterior eye diseases. *J Control Release*. Nov 10 2014;193:100-12. doi:10.1016/j.jconrel.2014.05.031
24. Wang Y, Shahi PK, Wang X, Xie R, Zhao Y, Wu M, Roge S, Pattnaik BR, Gong S. In vivo targeted delivery of nucleic acids and CRISPR genome editors enabled by GSH-responsive silica nanoparticles. *J Control Release*. Aug 10 2021;336:296-309. doi:10.1016/j.jconrel.2021.06.030
25. Sharma R, Khristov V, Rising A, Jha BS, Dejene R, Hotaling N, Li Y, Stoddard J, Stankewicz C, Wan Q, et al. Clinical-grade stem cell-derived retinal pigment epithelium patch rescues retinal degeneration in rodents and pigs. *Sci Transl Med*. Jan 16 2019;11(475)doi:10.1126/scitranslmed.aat5580
26. Richter MF, Zhao KT, Eton E, Lapinaite A, Newby GA, Thuronyi BW, Wilson C, Koblan LW, Zeng J, Bauer DE, et al. Phage-assisted evolution of an adenine base editor with improved Cas domain compatibility and activity. *Nat Biotechnol*. Jul 2020;38(7):883-891. doi:10.1038/s41587-020-0453-z
27. Park J, Lim K, Kim JS, Bae S. Cas-analyzer: an online tool for assessing genome editing results using NGS data. *Bioinformatics*. Jan 15 2017;33(2):286-288. doi:10.1093/bioinformatics/btw561

28. Clement K RH, Canver MC, Gehrke JM, Farouni R, Hsu JY, Cole MA, Liu DR, Joung JK, Bauer DE, Pinello L. CRISPResso2 provides accurate and rapid genome editing sequence analysis. *Nat Biotechnol*. 2019;37(3):224-226. doi:0.1038/s41587-019-0032-3

29. Kabra M, Moosajee M, Newby GA, Molugu K, Saha K, Liu DR, Pattnaik BR. Comprehensive Analysis of CRISPR Base Editing Outcomes for Multimeric Protein. *bioRxiv*. 2022:2022.06.20.496792. doi:10.1101/2022.06.20.496792

30. Hwang GH, Park J, Lim K, Kim S, Yu J, Yu E, Kim ST, Eils R, Kim JS, Bae S. Web-based design and analysis tools for CRISPR base editing. *BMC Bioinformatics*. Dec 27 2018;19(1):542. doi:10.1186/s12859-018-2585-4

31. Siegner SM, Karasu ME, Schroder MS, Kontarakis Z, Corn JE. PnB Designer: a web application to design prime and base editor guide RNAs for animals and plants. *BMC Bioinformatics*. Mar 2 2021;22(1):101. doi:10.1186/s12859-021-04034-6

32. Yin W, Kim HT, Wang S, Gunawan F, Wang L, Kishimoto K, Zhong H, Roman D, Preussner J, Guenther S, et al. The potassium channel KCNJ13 is essential for smooth muscle cytoskeletal organization during mouse tracheal tubulogenesis. *Nat Commun*. Jul 19 2018;9(1):2815. doi:10.1038/s41467-018-05043-5

33. Bae S, Park J, Kim JS. Cas-OFFinder: a fast and versatile algorithm that searches for potential off-target sites of Cas9 RNA-guided endonucleases. *Bioinformatics*. May 15 2014;30(10):1473-5. doi:10.1093/bioinformatics/btu048

34. Stenson PD, Ball EV, Mort M, Phillips AD, Shiel JA, Thomas NS, Abeysinghe S, Krawczak M, Cooper DN. Human Gene Mutation Database (HGMD): 2003 update. *Hum Mutat*. Jun 2003;21(6):577-81. doi:10.1002/humu.10212

Supplementary tables

Supplementary Table 1: Primers for in-fusion cloning of *KCNJ13* in FLP-In™ expression vector

Primer name	Sequence (5'-3')	GC %
In-fusion FP	TCACTATAGGGAGACCCAAGCTGGCTAGCGTTTAAACTTAatggtgagcaagggcgagga	50.0
In-fusion RP	AGTCGAGGCTGATCAGCGGGTTTAAACGGGCCCTCTAGACttattctgtcagtcctgttt	50.0
GFP FP	CAAGTCCGGACTCAGATCTCGAGCTC	57.1
Kir7.1 RP	TTATTCTGTCAGTCCTGTTT	72.7

FP: Forward primer, RP: Reverse primer. Primers for in-fusion cloning were designed using the Gibson assembly primer design tool available at https://tools.sgidna.com/gibson-assembly-primers.html and ordered from IDT (https://www.idtdna.com). The homology sequence is in uppercase, and the annealing sequence is in lowercase. The primers for Sanger sequencing (GFP FP and Kir7.1 RP) were designed using the NCBI Primer-BLAST tool (https://www.ncbi.nlm.nih.gov/tools/primer-blast/).

Supplementary Table 2: Primers to genotype mice

Primer name	Sequence (5'-3')	GC %
mKcnj13-FP	TAAATCAGCTACGGGCTAACA	42.86
mKcnj13-RP	CTGTGATAAAAGCCTCTAGCA	42.86

The primers were designed using the NCBI Primer-BLAST tool (https://www.ncbi.nlm.nih.gov/tools/primer-blast/). Annealing temperature 55 °C.

Supplementary Table 3: Primers to amplify the *hKCNJ13* on-target sites

Primer name	Sequence (5'-3')	GC %
NGS-hKCNJ13-FP	TCAAATGGATGGCGCTCAAAGA	45.0
NGS-hKCNJ13-RP	ATACCAGAGCACTGCAAAGACAA	43.0

The primers were designed using the NCBI Primer-BLAST tool and ordered along with an adaptor sequence for Illumina NGS platform from IDT. Adaptor sequence for FP: 5'-ACACTCTTTCCCTACACGACGCTCTTCCGATCT-3'Adaptor sequence for RP: 5'-GTGACTGGAGTTCAGACGTGTGCTCTTCCGATCT-3'.

Supplementary Table 4: Putative off-targets sites of human-sgRNA identified using Cas-OFFinder

S. No.	Location	Chr	strand	mismatches	G	C	G	C	T	A	G	C	G	T	T	G	G	A	T	G	A	T	G	T	T	G	G
1	STK24	13	-	3	·	T	·	·	·	·	·	·	C	·	·	·	·	·	·	·	T	·	·	·	G	G	G
2	GRCh38:13305873 2 Intergenic	10	-	3	·	·	A	·	G	·	·	G	·	·	·	·	·	·	·	·	·	·	·	·	T	A	G
3	GRCh38:50530925 Intergenic	18	-	2	·	G	·	·	·	·	C	·	·	·	·	·	·	·	·	·	·	·	·	·	C	A	G
4	PPM1K Intronic	4	+	3	·	·	·	A	G	·	·	·	T	·	·	·	·	·	·	·	·	·	·	·	T	G	G
5	AP2B1 Intronic	17	-	4	·	·	·	·	·	T	·	·	T	·	·	·	T	·	·	·	·	·	·	·	G	G	G
6	TMEM117 Intronic	12	+	4	·	·	·	·	·	T	T	·	T	·	·	T	·	·	·	·	·	·	·	·	T	G	G
7	GRCh38:113728054 Intronic	4	+	4	·	·	·	G	·	·	·	A	·	·	G	·	·	·	G	·	·	·	·	·	G	G	G
8	HRH1 Intronic	3	-	4	·	·	·	·	·	G	·	A	·	·	·	·	T	·	·	·	C	·	·	·	G	G	G
9	GRCh38:553528 15 Intergenic	12	-	3	·	·	·	·	·	·	·	·	T	A	·	·	·	T	·	·	·	·	·	·	T	G	G

Supplementary Table 5: Primers to amplify the off-target sites of human-sgRNA

S. No.	**Primer name**	**Sequence (5'-3')**	**GC %**
1	STK24_NGS_F	GGGATGCCACTTGGAGAACT	55.0
	STK24_NGS_R	ATTCTGGGTACACACTCCCA	50.0
2	ING_CHR10_NGS_F	CAGAGAGCTCCTTCTTTCTCTGA	47.83
	ING_CHR10_NGS_R	AAGCTCCTTCCCCAAGCAAA	50.0
3	ING_CHR18_NGS_F	TGTAATGGTGATCTAGTCACAGAG	41.67
	ING_CHR18_NGS_R	GCCTCATTCTGAAAGGGTCC	55.0
4	PPM1K_NGS_F	CCACTGCAGGTAGAGCTGTT	55.0
	PPM1K_NGS_R	CTGCACTCAAGCTGGGTTTC	55.0
5	AP2B1_NGS_F	TGAGCTCTTCCTGTAAGTGACC	50.0
	AP2B1_NGS_R	TGCATACCTTTGATGGCCTG	50.0
6	TMEM117_NGS_F	GTAGGTTCAATTTCTAACCCTTGC	55.0
	TMEM117_NGS_R	AGAGGAGAAATAGGAAGCAAAGT	55.0
7	INTRONIC_CHR4_NGS_F	TGAAGTCCAAGAAAAGGCAAA	38.0
	INTRONIC_CHR4_NGS_R	CCTCCCCAAACTGAATACAAAA	41.0
8	HRH1_NGS_F	GGGTACATGGCTATTGAGTAGG	50.0
	HRH1_NGS_R	GCCACCAGTTATGGCTCACT	55.0
9	ING_CHR12_NGS_F	CATGATAACTGTGGTGCGCT	50.0
	ING_CHR12_NGS_R	GTGACCTAAATCAGTTGGATGGAG	45.83

The primers were designed using the NCBI Primer-BLAST tool and ordered along with an adaptor sequence for Illumina NGS platform from IDT. Adaptor sequence for FP: 5'-ACACTCTTTCCCTACACGACGCTCTTCCGATCT-3'Adaptor sequence for RP: 5'-GTGACTGGAGTTCAGACGTGTGCTCTTCCGATCT-3'.

Supplementary Table 6: Potential off-target sites of mouse W53X-sgRNA identified using Cas-OFFinder

S. No	#Bulge type	crRNA	DNA	Chr	Position	Strand	Mismatches	Bulge Size
1	DNA	GCGCTAGCGCTGGAT-GATGCNRG	GCaCTAGgGCTGGATGGATGCAAG	chr5	27794505	-	2	1
2	X	GCGCTAGCGCTGGATGATGCNRG	GgtCcAGCGCaGGATGATGCTGG	chr2	30011064	+	4	0
3	RNA	GCGCTAGCGCTGGATGATGCNRG	GgGCgAGC-CTGGATGATGCTGG	chr2	74762664	-	2	1
4	RNA	GCGCTAGCGCTGGATGATGCNRG	GttCTAGC-CTGGATGATGCAAG	chr2	116880781	-	2	1
5	X	GCGCTAGCGCTGGATGATGCNRG	GCtCaAGCtCTGGtTGATGCCAG	chr17	47011867	+	4	0
6	X	GCGCTAGCGCTGGATGATGCNRG	GgGCTAGCGCTGGATGcTGCTGG	chr16	38496875	-	2	0
7	X	GCGCTAGCGCTGGATGATGCNRG	GCcCTcGgGaTGGATGATGCAAG	chr9	103261947	+	4	0
8	X	GCGCTAGCGCTGGATGATGCNRG	GtGCTAtCtCTaGATGATGCCAG	chr6	134150494	+	4	0

9	X	GCGCTAGCGCTGGATGATGCNRG	GCGCTAGCcCTGGATGgTGgTGG	chr11	97642214	-	3	0
10	X	GCGCTAGCGCTGGATGATGCNRG	GCtaTgGtGCTGGATGATGCTGG	chr3	28240364	+	4	0
11	DNA	GCGCTAGCGCT-GGATGATGCNRG	GCGCTAGCGCTGGGAgGgTGCTGG	chr7	93020838	-	2	1

Supplementary Table 7: sgRNA design using CRISPR-RGEN and PnB Designer

CRISPR Target (5'-3')	PAM	AA sequence	Direction	GC contents (% w/o PAM)
AACGC**T**AGCGCATGTCCATT	AGG	**C**AG **Q**	-	50.0
TAATGG**A**CATGCGCTAGCGT	TGG	ATGG**G**C M **G**	+	50.0
GCGCT**A**GCGTTGGATGATGT	TGG	T**G**G **W**	+	50.0

The sgRNAs were designed using CRISPR-RGEN tool available at http://www.rgenome.net. The letters highlighted in red are the targeted nucleotide base using the protospacer. Amino acids listed in blue would create a missense mutation, while in green would create the desired amino acid change to make a WT Kir7.1 protein.

Protospacer	PAM	EditPos.	Base.Editor
GCGCT**A**GCGTTGGATGATGT	TGG	6	ABEmax/ABE8e
ATGCGCT**A**GCGTTGGATGAT	GTTGGT	8	SaKKH-ABEmax/ABE8e

The sgRNAs were designed using PnB Designer available at https://fgcz-shiny.uzh.ch/PnBDesigner/. Letters highlighted in red are the targeted nucleotide base using the protospacer and BE.

Supplementary Table 8: sgRNA design for mouse *Kcnj13* using Benchling.

Strand	sgRNA	PAM	Purpose	On-target score	Off-Target score
+	GAATCCTAATGGACATGCGC	TGG	WT disruption	56.6	48.4
+	GCGCTAGCGCTGGATGATGC	TGG	W53X editing	57.1	82.9

Supplementary Figures

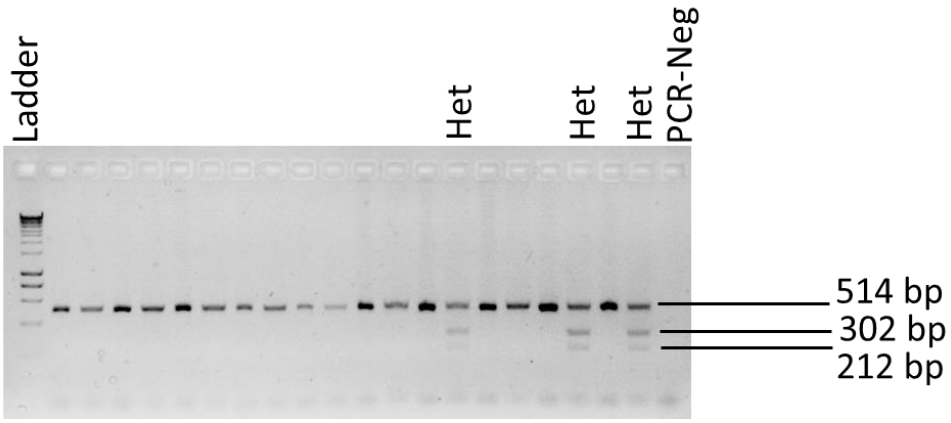

Supplementary Figure 1: Agarose gel electrophoresis showing the differences in W53X heterozygous and WT mice. *W53X mutation creates a restriction site for NheI; therefore, the W53X allele resulted in two (212 bp and 302 bp) fragments while the WT allele only one (514 bp) fragment.*

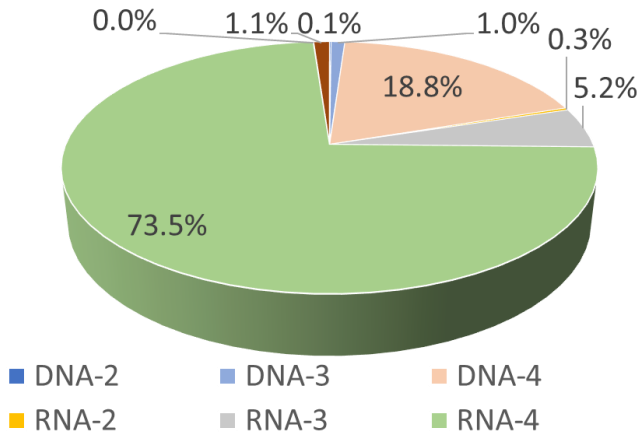

Supplementary Figure 2: Genomic off-target sites for human W53X sgRNA*. The sites were identified using standard criteria, up to 1-4 mismatches and DNA/ RNA bulge (size=1 nucleotide).*

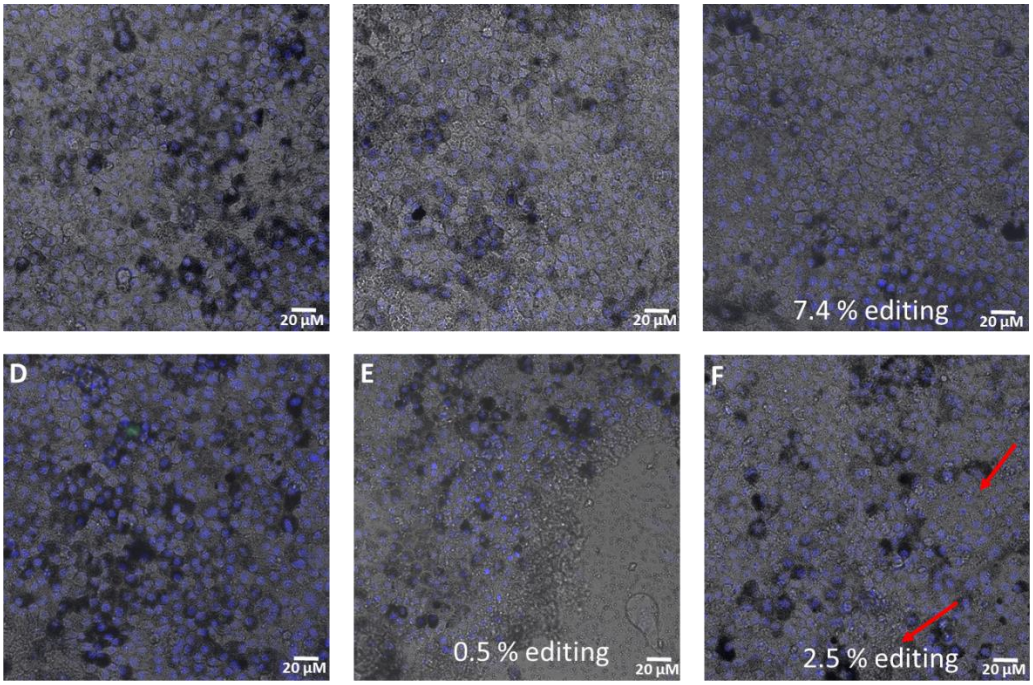

Supplementary Figure 3: Delivery of Different Doses and Concentration of RNP-Polyplex on Mature iPS-RPE Monolayer. *Mature iPS-RPE monolayer on transwell after the delivery of RNP-Polyplex complex. Hoechst stain (blue fluorescence) is used to label the nucleus of the live cell to test their health. A] Image of untreated iPS-RPE W53X control. B] Only donor (ssODN) was delivered using polyplex. C] single dose (Day 5). D] 2 doses (Day 3,5). E]3 doses (Day 1,3,5) 12µg of RNP-Polyplex was delivered to the W53X iPS-RPE. F] Single dose 16 µg of RNP-Polyplex was delivered before isolating the gDNA for NGS.*

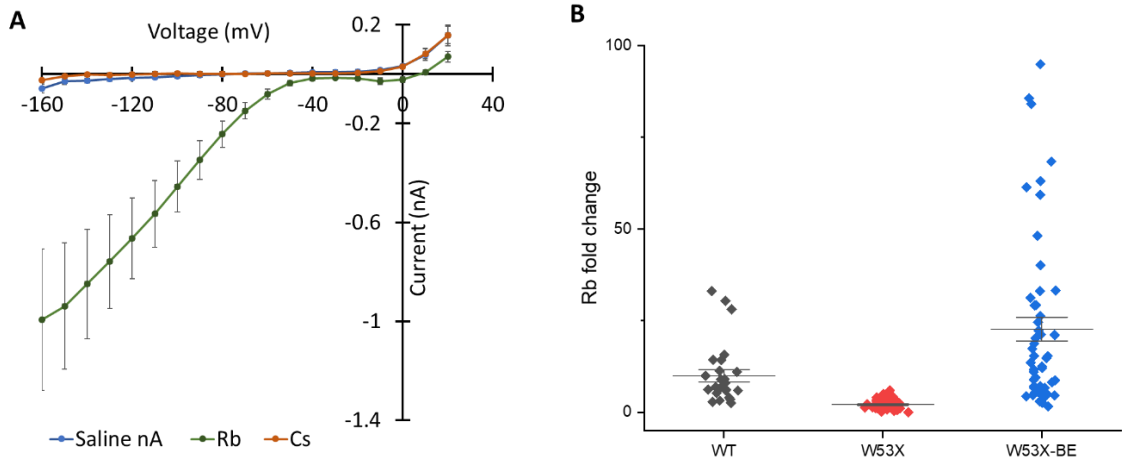

Supplementary Figure 4: Automated patch-clamp recordings from HEK^{W53X}, HEK^{WT,} and $^{HEKW53X\text{-}BE}$ cells. *A] I-V curve for HEK^{WT} cells showing a large negative membrane potential. B] The fold changes for Rb^{+} and Cs^{+} in HEK^{WT}, HEK^{W53X}, and $^{HEKW53X\text{-}BE}$ cells.*

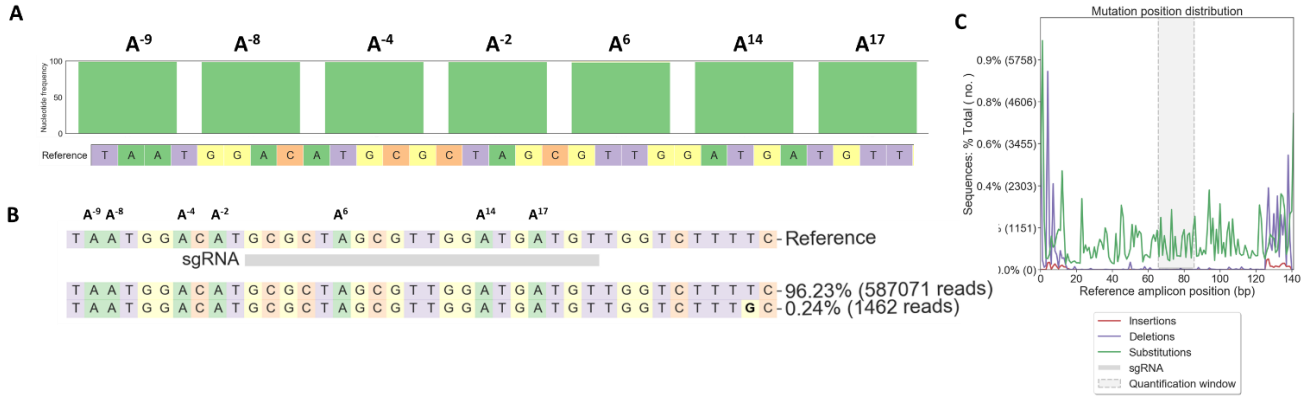

Supplementary Figure 5: Sequencing readouts from untreated LCA16-Fibroblasts^{W53X} used as reference. *A] Nucleotide distribution around sgRNA location as observed in sequencing reads. B] Percentage of sequencing reads observed in the untreated sample. C] Percentage distribution of substitution and deletion at sgRNA location.*

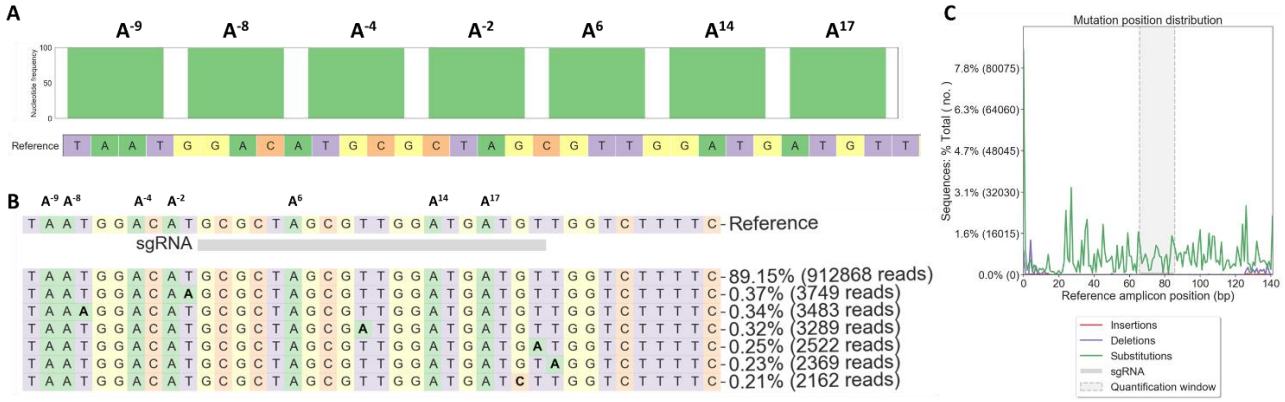

Supplementary Figure 6: Sequencing readouts from untreated iPSC RPE^{W53X} cells used as reference. *A] Nucleotide distribution around sgRNA location as observed in sequencing reads. B] Percentage of sequencing reads observed in the untreated sample. C] Percentage distribution of substitution and deletion at sgRNA location.*

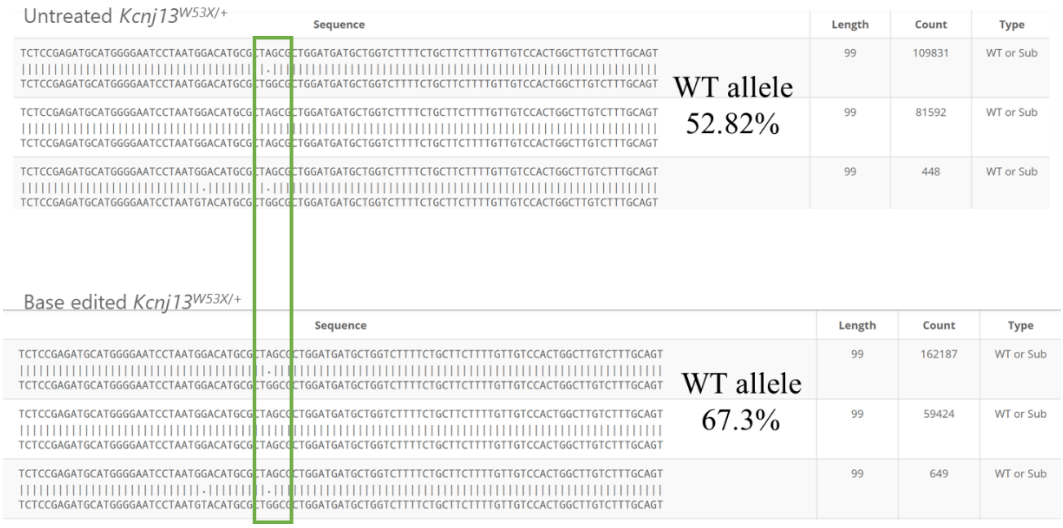

Supplementary Figure 7: Deep sequencing reads from the edited fibroblasts isolated from Kcnj13$^{W53X/-}$ mice. *The sequencing reads were generated by editing mouse W53X alleles within fibroblasts using ABE8e and W53X-sgRNA, delivered via nucleofection.*